A DRIVEN APPROACH TO PROPER VEHICLE MODELING AND MODEL VALIDATION

GREG BROWNE

A DRIVEN APPROACH TO PROPER VEHICLE MODELING AND MODEL VALIDATION

by

© Greg Browne

A thesis submitted to the

School of Graduate Studies

in partial fulfillment of the

requirements for the degree of

Master of Engineering

Faculty of Engineering and Applied Science

Memorial University of Newfoundland

May 2011

St. John's Newfoundland

Abstract

As the use of model-based design in the automotive industry accelerates, so must the efficiency of modeling techniques and the thoroughness of model validation.

The research presented constructs an energy-based (bond graph) proper vehicle model. This model includes all significant system dynamics generated from pressing on the gas pedal to the resulting vehicle translation.

The Model Order Reduction Algorithm provides a mechanism to quantitatively rank each element in the model and determine its contribution. The complete model, containing 65 elements, is reduced to 22 elements, provides simulation results of adequate agreement, and still contains over 98% of the original system energy. This proper model reduces the number of calculations by 86% and the simulation time by 92%.

By using GPS and OBD-II technologies, the model is exercised by logging on-road real-world vehicle data. By comparing the logged data to the predictions of the model, it is shown that $R^2 > 0.9$ can be achieved across different vehicles (compact sedan versus sport utility vehicle) and geographical routes.

Acknowledgments

Acknowledgement is made for the financial investment from the people and departments of Memorial University. In particular:

- Dr. Nicholas Krouglicof
- School of Graduate Studies
- Faculty of Engineering and Applied Science
- Graduate Students' Union

Appreciation is also given to Dr. Nicholas Krouglicof and Dr. Geoff Rideout for the contributions and advice they have given throughout the course of research.

Thanks are extended to Maurice Tuff and Root Four Imagination for allowing access to a beta version of their OSAPI™ OBD-II technology for use in the research described in Chapter 4.

Thanks are also extended to my family for providing one of the vehicles used for gathering the data presented in Chapter 4.

Acknowledgment is made to the Society of Automotive Engineers (SAE) for the publication of "An Energy-Based Proper Model of an Automotive Fuel Delivery System" (presented in Chapter 2) and to the Institute of Electrical and Electronics Engineers (IEEE) for the publication of "Pedal to Pavement: An Energy-Based Proper Vehicle Model" (presented in Chapter 3).

Table of Contents

List of Tables

List of Figures

List of Appendices

Chapter 1 Introduction

Proper vehicle modeling, proper modeling techniques, and model validation are becoming more important topics of discussion in the automotive industry. Some of the largest automobile manufacturers are moving towards model-based design as their tool-of-choice for new development.

For example, Toyota was one of the first manufacturers to adopt model-based design through its entire development cycle [1]. General Motors used model-based design to develop their Two-Mode Hybrid (combination of internal combustion engine and dual electric motors) powertrain [2]. Ford Motor Company used model-based design for the development of the control software for the battery management system of the 2010 Ford Fusion Hybrid [3].

Considering the potential in this field to the automotive industry, the research presented in this thesis aims to illustrate the proper modeling process by building a proper vehicle model and validating the model using novel on-road techniques.

1.1 Proper Modeling Process

Given the accelerating adoption rate of model-based design, it is critical that guidelines be put in place to ensure that proper modeling techniques result in accurate models. A standardized modeling procedure is the basis for quality assurance in a model-based design environment. The proper modeling process used throughout the research presented in this thesis is illustrated in Figure 1-1.

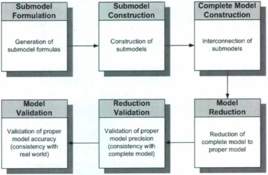

Figure 1-1 Steps to Proper Modeling

Submodel Formulation involves the identification and mathematical formulation of the physical equations that govern the dynamic behavior of the given submodel.

Submodel Construction involves the graphical layout of the elements of a submodel that implement the equations determined during *Submodel Formulation*. In the case of the research described in this thesis, submodels are constructed using bond graphs. Alternatively, one could construct submodels using block diagrams, if desired.

Complete Model Construction involves the interconnection of the submodels resulting from *Submodel Construction* (i.e. the connection of the input(s) and output(s) of neighboring submodels).

Model Reduction involves the systematic removal of elements from the model resulting from the *Complete Model Construction* in order to optimize the efficiency of the model. A *proper model* is achieved if it has minimal complexity, physically meaningful parameters, and accurately predicts dynamic system responses [4]. In the case of the research described in this thesis, the Model Order Reduction Algorithm (MORA) is used for the model reduction process.

Reduction Validation involves the validation of the precision of the reduced model obtained during *Model Reduction* (i.e. that the reduced model provides the same simulation results as the complete model). Various statistical techniques and/or tools may be used for this validation process.

Model Validation involves the validation of the accuracy of the reduced model obtained during *Model Reduction* (i.e. that the reduced model provides simulation results that match actual real-world responses of the system being modeled). Various statistical techniques and/or tools may be used for this validation process.

1.2 Modeling Technique – Bond Graphs

Using the proper modeling process described in the previous section, bond graphs were used as the means of modeling described in this thesis. A discussion of bond graphs and their usage is given in the following sections.

1.2.1 Overview of Bond Graphs

In bond graphs [5], generalized inertias I and capacitances C store energy as a function of the system state variables, which are generalized momenta and displacements. The time derivatives of generalized momentum p and displacement q are generalized effort e and flow f, the product of which is power. Generalized resistors R remove energy from the system, and have a constitutive law relating generalized effort to generalized flow. Sources of effort and flow (*Se* and *Sf*) represent ports through which the system interacts with its environment.

Energy is transported among source, storage and dissipative elements through power-conserving "junction structure" elements. Such elements include power-continuous generalized transformers (*TF*) and gyrators (*GY*) that algebraically relate elements of the effort and flow vectors into and out of the element. The constitutive laws of "modulated" transformers and gyrators (*MTF* and *MGY*) are functions of external variables, for example coordinate transformations that are functions of generalized coordinates. Kirchoff's loop and node laws are modeled by power-conserving 1- and 0-junctions, respectively. Elements bonded to a 1-junction have common flow, and their efforts algebraically sum to zero. Elements bonded to a 0-junction have common effort, and their flows algebraically sum to zero.

The power bonds contain a half-arrow that indicates the direction of algebraically positive power flow, and a causal stroke normal to the bond that indicates whether the effort or flow variable is the input or output from the constitutive law of the connected element. Full arrows are reserved for modulating signals that represent powerless information flow, such as orientation angles for coordinate transformation matrices [6].

It is important to note that this thesis also contains pseudo-bond graphs, indicated by dashed bonds. A pseudo-bond graph typically has one or both of its effort-flow pairs that are a variant of the standard quantity, whereby the product is not power. This is not uncommon when dealing with compressible gas dynamics[7] where it is more convenient to deal with the gas flow in terms of mass flow (kg/s) instead of the standard volumetric flow rate (m^3/s). Re-introduction into standard bond graphs is accomplished by means of a transformer, with the gas density as the modulus.

Appendix A defines the symbols and constitutive laws for energy storage and dissipative elements ("energetic" elements), sources, and power-conserving elements. The constitutive laws are written in an input-output form consistent with the placement of the causal strokes. The reader is referred to [7] for a more thorough development of bond graphs.

1.2.2 Why Bond Graphs?

The more typical method of modeling uses block diagrams, such as the block diagram of an engine model (implemented in *Simulink*), shown in Figure 1-2. However, the research presented in this thesis uses bond graphs instead of block diagrams, for the reasons discussed in the following sections.

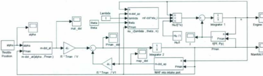

Figure 1-2 Engine Model Block Diagram

1.2.2.1 Analogous Structures

All bond graph elements (energy dissipation, storage, transformation, etc) have the same structure, regardless of the energy domain they are representing. Consider the 1-junction bond graph shown in Figure 1-3 that connects a resistive and inertial element. As illustrated, this bond graph could represent an electrical R-I branch (like a motor winding), a hydraulic pipe segment, or a mass-damper system.

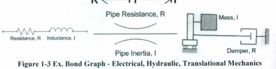

Figure 1-3 Ex. Bond Graph - Electrical, Hydraulic, Translational Mechanics Domains

This enables the model-based designer to easily make analogous interpretations of the subsystems based on the domain in which they feel most comfortable.

1.2.2.2 Interconnectivity

Because bond graphs share a common structure and set of elements, it is easily seen that the interconnection of subsystems across different domains is seamless (as is the case in the real physical world). Furthermore, when analyzing a bond graph model, one can easily identify the transition(s) between domains by locating the energy transformation elements (i.e. transformers and/or gyrators). This transition may be "lost in the math" for traditional block diagrams or numerical models.

1.2.2.3 Physical Connections

The bonds in bond graphs are more physically meaningful (containing both effort and flow information) rather than simply flow of data between units of computation [8], as is the case with traditional block diagrams. This results in a model which is more easily interpreted, as well as the benefits described in the previous and following sections.

1.2.2.4 Efficient Model Reduction

Because the bond from each element contains power information, reduction algorithms such as the Model Order Reduction Algorithm (MORA)[4] can be utilized to efficiently analyze the contribution of each element. This allows elements to be quantitatively eliminated, thereby removing the guesswork. Model reduction using MORA is discussed in further detail in Chapter 2 and Chapter 3.

1.3 Literature Review

When considering the application of the proper modeling process discussed in this chapter to an automotive application, one must consider the prior contributions and discussions within the related industries. The contributions and discussions applicable to the research presented in this thesis tend to fall into one of the following categories:

1. Partial Vehicle Models
2. Complete Vehicle Models
3. Automotive Model Validation Techniques

The literature pertaining to each of the above categories is discussed in the following sections.

1.3.1 Partial Vehicle Models

It is not unreasonable to expect that much of the existing literature will be focused around partial vehicle models, wherein the research of the author(s) is based primarily on a single subsystem of a vehicle.

On the input side of a vehicle model is the fuel delivery system. In [9], Wu *et al* construct a numerical model of a fuel rail system (fuel injectors, pressure regulator, pressure damper, fuel pump, and fuel supply/return lines), based on Figure 1-4. Their research was based on the investigation of pressure fluctuations and its relation to fuel rail system geometry.

In [10], Yang *et al* construct a bond graph model similar to the fuel rail system of Wu *et al* (except the pressure damper). Their research was centered on the characterization of pressure transients based on the chemical distribution inside the fuel rail.

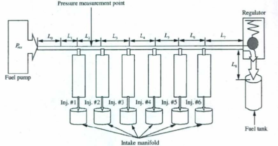

Figure 1-4 Wu *et al* Fuel Rail System Schematic

On the output side of a vehicle model is the suspension system. In [11], Adibi-asl and Rideout build a hybrid bond graph and block diagram model of a vehicle suspension system with seven degrees-of-freedom. Their research was conducted to investigate the benefits of active suspension in contrast to passive suspension systems.

In [12], Ozkan *et al* construct a bond graph suspension model, based on Figure 1-5, and also a block diagram controller output observer for output estimation. Their research was focused on the use of the controller output observer as a means of estimating vehicle tire forces.

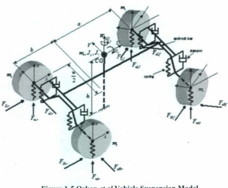

Figure 1-5 Ozkan *et al* Vehicle Suspension Model

Mean Value Engine Models (MVEMs) have been of particular interest to engine designers and emission testers as a way to apply a generic mathematical umbrella to the variety of engine permutations in the industry. In [13], Hendricks *et al* construct an MVEM using block diagrams, which is expanded upon in [14]. Their research was intended to establish, and expand upon, the concept of MVEMs.

In [15], Karmiggelt builds a numerical MVEM, based on Figure 1-6, with the intention of connecting the model outputs to a continuously variable transmission (CVT) model for the purpose of analyzing the fuel efficiency of a proposed hybrid driveline.

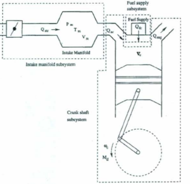

Figure 1-6 Karmiggelt MVEM Schematic

1.3.2 Complete Vehicle Models

Complete vehicle models, such as the one presented in this thesis, aim to model the complete set of interactions between vehicle subsystems and, potentially, between the vehicle and the external environment.

In [16], Hedrick *et al* build a three-state and four-state numerical model of a complete vehicle, with focus on the engine, transmission, and driveline. Their research was aimed at producing an accurate vehicle model to be used in controller design for autonomous vehicles, following either a spacing or headway control algorithm.

In [17], Filippa *et al* construct a complete vehicle and test cell model, shown in Figure 1-7. Using a simplified powertrain model, their research was focused on the development of a test cell to be used for the load testing of Hybrid Electric Vehicle (HEV) powertrains.

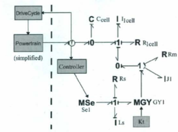

Figure 1-7 Filippa *et al* Test Cell Model

1.3.3 Automotive Model Validation Techniques

When considering the proper modeling process, equal importance must be given to the model validation steps. Without ensuring the accuracy and integrity of a model, no confidence can be given to its performance in model-based design.

With regards to most partial vehicle models, it is often the case that a test bench may be constructed to validate the model. Such is the case with [9] and [10] whereby the authors constructed a replicated test bench setup of a fuel rail system to measure pressure responses to simulated inputs.

When validating an MVEM or complete vehicle model, more often than not, a dynamometer (dyno) is used, as is the case with [13]. A dyno is a piece of specialized equipment used for torque-speed characterization. Depending on the application and dyno, characterization can either be made at the crankshaft or at the vehicle wheels.

A more novel vehicle model validation technique is described in Chapter 4, as part of the research presented in this thesis.

1.4 Co-Authorship Statements

The sections below discuss the contributions of each author to the research presented in the chapters to follow. The sections mostly discuss the contributions of the co-authors other than the thesis author, with the intention that the unmentioned contributions were completed by the thesis author in whole.

1.4.1 Co-Author Contributions – Chapter 2

Chapter 2 presents "An Energy-Based Proper Model of an Automotive Fuel Delivery System", a conference paper published by SAE International. The initial design and model construction was composed by the thesis author as the project requirement for a graduate course taught by Dr. Rideout, "Modeling and Simulation of Dynamic Systems". Following the completion of the course, both Dr. Rideout and Dr. Krouglicof were involved in discussions regarding how to improve the model. Furthermore, Dr. Krouglicof contributed significantly to the *Submodel Formulation* and *Submodel Construction* steps and Dr. Rideout to the *Complete Model Construction* and *Model*

Reduction steps (see Figure 1-1). The majority of the paper was written by the thesis author, with contributions and review from both Dr. Krouglicof and Dr. Rideout.

1.4.2 Co-Author Contributions – Chapter 3

Chapter 3 presents "Pedal to Pavement: An Energy-Based Proper Vehicle Model", a conference paper in print (at the time of thesis submission) by the IEEE. Design decisions were discussed between the thesis author and Dr. Krouglicof. Dr. Krouglicof contributed significantly to the *Submodel Formulation* and *Submodel Construction* steps (see Figure 1-1). The majority of the paper was written by the thesis author, with advice and review from Dr. Krouglicof.

1.4.3 Co-Author Contributions – Chapter 4

Chapter 4 presents "A Proper Vehicle Model Road Test: Real-World Model Validation", a (potential) journal article under review (at the time of thesis submission). Design decisions were discussed between the thesis author and Dr. Krouglicof. Hardware and software were mostly designed by the thesis author, with advice and review from Dr. Krouglicof. Dr. Krouglicof contributed to the data analysis in the *Model Validation* step (see Figure 1-1). The majority of the paper was written by the thesis author, with advice and review from Dr. Krouglicof.

Chapter 2 An Energy-Based Proper Model of an Automotive Fuel Delivery System

2.1 Introduction

Any design expert in the automotive industry will most likely use some form of mathematical modeling when analyzing a product or procedure. An accurate mathematical model is essential in determining the response of a system and reviewing its characteristics.

Bond graphs are an efficient way of describing multiport systems, in that the connections (bonds) between system elements have both an effort and a flow whose product is the power of the bond [7]. Moreover, bond graphs allow for the seamless interconnection of systems across energy domains (hydraulics, rotational mechanics, translational mechanics, electrodynamics, etc). Therefore, bond graphs are used as the preferred means of modeling presented in this chapter.

The main subsystems of an automotive fuel delivery system are shown as a block diagram in Figure 2-1.

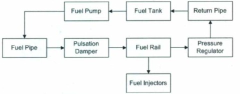

Figure 2-1 Fuel Delivery System Block Diagram

2.2 Model Construction

To better understand the characteristics of the fuel delivery system, the subsystems can be generalized by their basic elements – shown as a schematic in Figure 2-2.

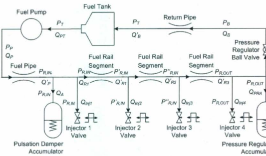

Figure 2-2 Fuel Delivery System Schematic

The variables illustrated in Figure 2-2 are used in the equations and derivations to follow.

Each subsystem can then be modeled individually based on the schematic. These subsystems are described in the following sections.

For quick reference, a table of bond graph elements can be found in Appendix A. For a more detailed description of bond graph formalism, the reader is referred to [7].

2.2.1 Fuel Tank

The simple function of the fuel tank is to store the fuel to be used by the system. Fuel is stored under slightly pressurized conditions, P_T, until it is drawn by the fuel pump. Unused fuel is returned to the tank via the return pipe.

The bond graph model for the fuel tank is shown in Figure 2-3.

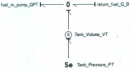

Figure 2-3 Fuel Tank Submodel

The *q-sensor* is used to calculate the current tank volume by subtracting the amount of fuel used by the pump and re-accumulating the returned fuel to the initial volume, $V_T(0)$. This relationship is shown in (2-1).

$$V_T = V_T(0) + \int (Q'_B - Q_{PT})\, dt \tag{2-1}$$

2.2.2 Fuel Pump

The fuel pump (either in-tank or in-line) draws fuel from the fuel tank to be delivered to the system via the fuel pipe. Classically, a pump is modeled as an ideal flow source, Q_{PT}, with some internal leakage proportional to the pressure across the pump, P_P [18]. This relationship is shown in (2-2).

$$Q_P = Q_{PT} - C_P P_P \tag{2-2}$$

Where, Q_P is the actual fuel flow delivered by the pump and C_P is the inherent leakage coefficient of the fuel pump (indicative of its volumetric efficiency).

This relationship is represented in bond graph form as illustrated in Figure 2-4.

Figure 2-4 Fuel Pump Submodel

2.2.3 Fuel Pipe

The fuel pipe delivers fuel from the fuel pump to the fuel rail. As fuel enters the fuel pipe, there will be an apparent loss in fluid flow due to its compressibility (bulk modulus, β), which is given by (2-3) [18].

$$\beta = -V_P(0)\frac{\partial P_P}{\partial V_P} \tag{2-3}$$

Where, V_P is the volume of fuel in the fuel pipe.

The resulting fuel flow undergoes a pressure drop associated with the inertia, I, and resistance, R, of the fuel pipe, before being delivered to the fuel rail. The pressure drop due to pipe inertia is given by (2-4).

$$\Delta P = I\dot{Q} = \frac{\rho l}{A}\dot{Q} = \frac{4\rho l}{\pi D^2}\dot{Q} \tag{2-4}$$

Where, ρ is the density of gasoline, l and D are the length and diameter of the fuel pipe, respectively.

The pressure drop due to the resistance of a pipe is non-linear, given by (2-5).

$$\Delta P = RQ^2 \tag{2-5}$$

Furthermore, the resistance of a pipe varies based on the nature of the fluid flow that passes through it (determined by its Reynolds Number, Re). This piece-wise relationship is given by (2-6).

$$R = \begin{cases} \dfrac{32 v l \rho}{AD^2}, & Re \leq Re_L \\ \left[\dfrac{64}{Re_L} + \left(\dfrac{0.3164}{Re_T^{0.25}} - \dfrac{64}{Re_L}\right)\left(\dfrac{Re - Re_L}{Re_T - Re_L}\right)\right]\dfrac{\rho l A^2}{2D}, & Re_L < Re < Re_T \\ \left(\dfrac{0.3164}{Re^{0.25}}\right)\dfrac{\rho l A^2}{2D}, & Re \geq Re_T \end{cases} \tag{2-6}$$

Where, v is the viscosity of gasoline, A is the cross-sectional area of the fuel pipe, Re_L is the maximum Reynolds number for laminar fluid flow, and Re_T is the minimum Reynolds number for turbulent flow. The first part of the expression is the relationship for pipe flow with laminar flow, the last part is for turbulent flow [18], and the middle part is a linear interpolation function [19].

The Reynolds Number is calculated using (2-7).

$$Re = \frac{QD}{vA} \tag{2-7}$$

By combining (2-3) to (2-7), a relationship can be derived for output pressure, P_{out}, given by (2-8).

$$P_{out} = \frac{\beta}{V_P(0)} \int Q\,dt - \frac{4\rho l}{\pi D^2}\dot{Q} - RQ^2 \tag{2-8}$$

This relationship is represented in bond graph form as illustrated in Figure 2-5.

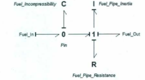

Figure 2-5 Fuel Pipe Submodel

2.2.4 Pulsation Damper

The pulsation damper acts as an accumulator to smooth out the small drops in pressure created by the injectors during their firing sequence [20]. However, not all vehicles utilize a pulsation damper and instead rely on the fuel pressure regulator to account for any fluctuations in pressure as best it can.

A bolt is attached to a diaphragm that moves with changes in fuel pressure, $P_{R,in}$. This relationship is shown as (2-9).

$$P_{R,in} - P_{atm} = \frac{k_A}{A_A} \int Q_A \, dt \tag{2-9}$$

Where, P_{atm} is atmospheric pressure (101.325 kPa), k_A is the stiffness of the bolt/diaphragm assembly (the inverse of the compliance, C_A), A_A is the cross-sectional area of the pulsation damper, and Q_A is the fuel flow into the pulsation damper.

This relationship is represented in bond graph form as illustrated in Figure 2-6.

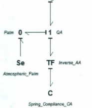

Figure 2-6 Pulsation Damper Submodel

2.2.5 Fuel Rail

The fuel rail is a pipe that delivers fuel to each of the fuel injectors (Q_{inj1} through Q_{inj4}). Unused fuel is returned to the fuel tank via the return pipe.

The piping between each injector will have restrictive effects similar to that discussed in the Fuel Pipe section – a change in fluid flow due to its compressibility (bulk modulus) and a pressure drop due to the inertia and resistance of the pipe segment.

The bond graph for the fuel rail is given in Figure 2-7.

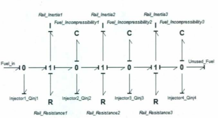

Figure 2-7 Fuel Rail Submodel

2.2.6 Fuel Injectors

The fuel injectors take fuel from the fuel rail, atomize it, and spray it directly into the intake manifold of their respective cylinder.

A fuel injector consists of a solenoid-actuated pintle or needle valve [10] that is controlled by the vehicle ECU (Electronic Control Unit). The injected fuel flow, Q_{inj}, from the injector is given by (2-10).

$$Q_{inj} = \begin{cases} C_d A_V \sqrt{\frac{2}{\rho}(P_R - P_{man})}, & ON \\ 0, & OFF \end{cases} \tag{2-10}$$

Where, C_d is the internal discharge coefficient of the injector valve, A_v is the cross-sectional area of the injector valve, P_R is the rail pressure at the given injector, and P_{man} is the manifold pressure (MAP).

The *ON* condition in (2-10) deals with the two main factors that control the fuel injection – timing and quantity.

Some vehicles utilize "simultaneous fuel injection" whereby, at a given series of crank angles, all fuel injectors fire at the same time and for the same duration. This is a less interesting injection pattern and, hence, will not be discussed.

The most common type of electronic fuel injection (EFI) is "sequential fuel injection" (SFI). This is a more robust scheme, illustrated by example in Figure 2-8, whereby at four different crank angles a single injector fires. This allows the system to make adjustments to fuel metering more quickly [20].

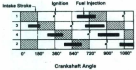

Figure 2-8 Sequential Fuel Injection (SFI) Pattern [20]

The assumption is that each injector has a baseband crank angle, θ_B, at which, for all multiples of this angle, the given injector will fire. For simulation, these are assumed to be 180° for injector 1, 720° for injector 2, 360° for injector 3, and 540° for injector 4 (based loosely on Figure 2-8).

It is also assumed that, at each particular triggering crank angle, the fuel injected will be half completed (i.e. the pulsed fuel will be centered about this trigger point).

The crank angle, θ_C, in degrees, can easily be derived from the engine RPM, as given by (2-11).

$$\theta_C = \frac{360}{2\pi}\int \left(\frac{2\pi}{60}\right) RPM\, dt = 6\int RPM\, dt \tag{2-11}$$

The quantity of fuel to be injected is converted to a pulse width, t_{ON}, during which the given injector is to fire. For a given load and negligible fuel trim, t_{ON} can be determined using (2-12).

$$t_{ON} = \frac{60(MAF)}{n_S R_{AF} \dot{m}_I (RPM)} \tag{2-12}$$

Where, MAF is the mass air flow rate (g/s), n_S is the number of strokes per revolution, R_{AF} is the air-fuel ratio, and $\dot{m}_I$ is the maximum fuel mass flow rate of the fuel injector (g/s).

However, the injection pattern is time-independent; therefore, it is more appropriate to express the fuel injection in terms of crank position. Therefore, the number of degrees the injector should fire per piston stroke, θ_{ON}, can be calculated using (2-13) (by multiplying the pulse width, given in (2-12), by the engine speed in deg/s).

$$\theta_{ON} = \frac{360(MAF)}{n_S R_{AF} \dot{m}_I} \tag{2-13}$$

For vehicles that do not have direct access to MAF (i.e. no MAF sensor is present), it is calculated by the ECU using (2-14) [21].

$$MAF = \frac{(MAP)(RPM)}{60 R_{air} T_{IA}} \left(\frac{V_{eng}}{2}\right) \tag{2-14}$$

Where, R_{air} is the specific gas constant for dry air, T_{IA} is the intake air temperature, and V_{eng} is the engine displacement (halved due to half the volume being swept during each revolution).

Considering (2-11) and (2-13), (2-10) can be re-written as (2-15).

$$Q_{inj} = \begin{cases} C_d A_V \sqrt{\frac{2}{\rho}(P_R - P_{man})}, & \left|\frac{\theta_{ON}}{2}\right| \leq (\theta_C \bmod 900) - \theta_B \\ 0, & otherwise \end{cases} \tag{2-15}$$

A fuel injector is represented in bond graph form as illustrated in Figure 2-9.

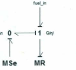

Figure 2-9 Fuel Injector Submodel

2.2.7 Fuel Pressure Regulator

The fuel pressure regulator is a diaphragm-operated pressure relief valve that maintains a constant pressure differential across the fuel injectors [10]. This is accomplished by means of a ball valve, which is held in place by a preloaded spring against a diaphragm [20]. The regulated fuel rail pressure, $P_{R,out}$, is given by (2-16).

$$P_{R,out} = P_{R,in} - P_{man} - \frac{\rho}{2}\left(\frac{Q_{out}}{2\pi r_{out} x_R C_B}\right)^2 \tag{2-16}$$

Where, $P_{R,in}$ is the pressure of the fuel as it enters the pressure regulator, Q_{out} is the fuel out of the pressure regulator (given by (2-17)), r_{out} is the output radius of the pressure regulator, x_R is the displacement of the spring (the solution to the ODE given by (2-18)), and C_B is the discharge coefficient of the ball valve.

$$Q_{out} = Q_R - A_R \dot{x}_R \tag{2-17}$$

Where, Q_R is the fuel flow into the pressure regulator and A_R is the effective area of the pressure regulator that can be filled with fuel.

$$k_R x_R + B_R \dot{x}_R + M_R \ddot{x}_R = A_{RP}\left(P_{R,in} - P_{man}\right) - F_0 \tag{2-18}$$

Where, k_R is the pressure regulator spring stiffness, B_R is the viscous damping resulting from the volume of fuel present in the regulator, M_R is the mass of the regulator, A_{RP} is the effective area upon which pressure is exerted, and F_0 is the preload on the spring.

The bond graph representation of the fuel pressure regulator is given in Figure 2-10.

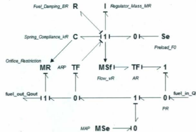

Figure 2-10 Fuel Pressure Regulator Submodel

2.2.8 Return Pipe

The return pipe delivers the fuel from the pressure regulator back to the fuel tank to be recirculated by the system. The return pipe has the same submodel as previously discussed in the Fuel Pipe section.

2.2.9 Submodel Interconnection

Due to the nature of bond graphs, the submodels can be easily interconnected to form the complete model previously outlined in the fuel delivery system schematic (Figure 2-2). This complete model is shown in Figure 2-11.

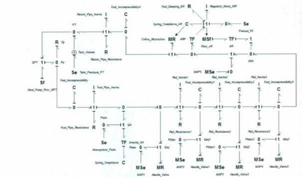

Figure 2-11 Fuel Delivery System Complete Model

2.3 Model Simulation

Model construction and simulation is implemented in the software package *20-Sim*.

All system parameters used for simulation are given in Appendix B.

The required inputs to the model in order to produce a representative system response are manifold air pressure (MAP), engine RPM, and mass air flow (MAF). As previously discussed, MAF is either available directly or calculated using the previous two inputs in conjunction with intake air temperature (IAT).

In order to achieve the most accurate results, data was logged directly from a vehicle (2004 Chevrolet Optra) using a previously developed OBD-II hardware and software interface [22].

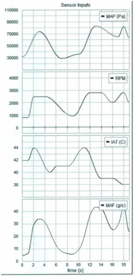

Figure 2-12 Sensor Inputs

Logged sensor inputs were emulated as shown in Figure 2-12. In this case, the Optra did not have a MAF sensor; therefore MAF was calculated as described in (2-14).

The resulting pressure responses of interest are shown in Figure 2-13.

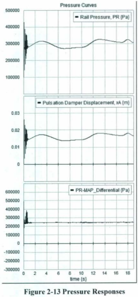

Figure 2-13 Pressure Responses

One can see the pulsation damper accumulator displacement, x_A, acting in response to fluctuations in rail pressure, P_R.

The resulting flow responses of interest are shown in Figure 2-14.

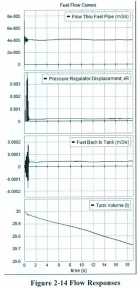

Figure 2-14 Flow Responses

One can see the pressure regulator displacement, x_R, acting to maintain a constant differential between rail and manifold pressure (shown in Figure 2-13). Also, it is shown that the fuel volume in the tank decreases, as expected, from an (arbitrary) initial volume of 30 L.

The initial transients are present for approximately the first second of simulation, and are better illustrated in Figure 2-15 (transient pressure responses) and Figure 2-16 (transient flow responses).

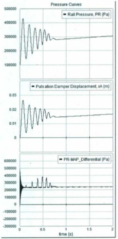

Figure 2-15 Transient Pressure Responses

Any model used to describe a similar fuel injection system should aim to accurately reproduce the transients and steady-state responses, depending on the application.

Therefore, any elements that do not have an effect on these responses can effectively be removed without adversely changing the behavior of the system.

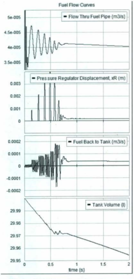

Figure 2-16 Transient Flow Responses

2.4 Model Reduction

By utilizing a method that quantizes the contribution of each element, one can make an informed decision regarding which elements to retain and which to eliminate from a proper model. A proper model has minimal complexity, physically meaningful parameters, and accurately predicts dynamic system responses [4].

The Model Order Reduction Algorithm (MORA) uses activity, A_i, to quantize the contribution of a given element. Activity is "absolute energy" and, for a given element *i*, is calculated by (2-19) [4].

$$A_i = \int |P_i(t)|\, dt \tag{2-19}$$

Where, P_i is the instantaneous power of element *i*.

Each element is assigned a non-dimensional activity index, AI_i, which is its fraction of the total system activity. For a given element *i* of *k* elements, its activity index is calculated using (2-20) [4].

$$AI_i = \frac{A_i}{A_{Total}} = \frac{\int |P_i(t)|\, dt}{\sum_{i=1}^{k}\{\int |P_i(t)|\, dt\}} \tag{2-20}$$

Activity indices are then sorted and elements eliminated from the lower end until the minimum number of elements required to satisfactorily reproduce the responses of the complete model is achieved.

2.4.1 Element Elimination

Element activities and activity indices resulting from the simulations are given in Appendix C.

2.4.1.1 99% Model

By following the MORA algorithm to achieve a 99% model (a model that still retains at least 99% of the activity of the complete model), the following elements were eliminated:

- Needle Valves for Injectors 1 through 4
- Fuel Pipe Resistance
- Pressure Regulator Fuel Damping
- Return Pipe Resistance
- Fuel Pipe Fuel Incompressibility
- Fuel Pipe Inertia
- Fuel Rail Resistance 1 and 3

However, by strictly following the algorithm, one can see in the transient plots, Figure 2-17 and Figure 2-18 that the system responses acquire a high frequency infection and become less damped than the complete model.

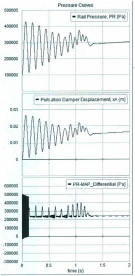

Figure 2-17 99% Model Transient Pressure Responses

High frequency infection is particularly noticeable in the pressure differential maintained by the pressure regulator (Figure 2-17) as well as the fuel back to tank (Figure 2-18).

The decrease in system damping is prevalent in each response shown.

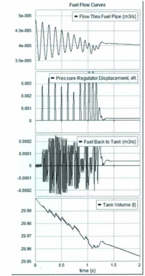

Figure 2-18 99% Model Transient Flow Responses

However, if the fuel damping in the pressure regulator, B_R, is reinstated, the system responses can be returned to an adequate representation of the responses of the complete model.

This decision also has a physically intuitive basis – there must be some damping present in the mass-spring subsystem of the pressure regulator to prevent it from continuing to oscillate beyond a reasonable time constant.

2.4.1.2 98% Model

While maintaining B_R, the model can be further reduced to 98% by removing the following elements:

- Fuel Rail Resistance 2
- Pressure Regulator Mass, M_R

The transient responses of this 98% model are shown in Figure 2-19 and Figure 2-20.

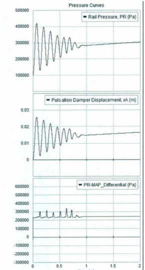

Figure 2-19 98% Model Transient Pressure Responses

By comparing the transient pressure responses of the 98% model (Figure 2-19) to that of the complete model (Figure 2-15) one can see that the rail pressure, P_R, and the pulsation damper displacement x_A, are certainly replicated. The differential between P_R and MAP is fairly well replicated; however, the initial 4.7 kHz harmonic is missing from the 98% model. The suitability of this model will be based on the given application.

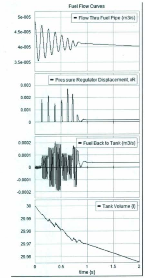

Figure 2-20 98% Model Transient Flow Responses

By comparing the transient flow responses of the 98% model (Figure 2-20) to that of the complete model (Figure 2-16) one can again see that the 98% model is still a relatively accurate representation of the complete system. Yet again the suitability would have to be determined by the given application.

2.4.1.3 97% Model

To further reduce the model to 97% of the original system activity would require the elimination of the following element:

- Pressure Regulator Spring Stiffness, k_R

Eliminating k_R effectively adds infinite stiffness to an already massless diaphragm assembly in the pressure regulator. When considering the rail pressure differential transient, the system is now incapable of effectively responding with the proper overshoot, as shown in Figure 2-21 (compared to Figure 2-19).

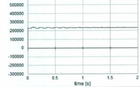

Figure 2-21 97% Model Rail Pressure Differential Transient Response

Furthermore, the output fuel flow from the pressure regulator, given by (2-17), was originally constrained by (2-18). For the 97% model, (2-18) becomes (2-21).

$$B_R \dot{x}_R = A_{RP}\left(P_{R,in} - P_{man}\right) - F_0 \tag{2-21}$$

This implies that any fluctuation in rail pressure, P_R, will cause an instantaneous change in the output flow from the pressure regulator. This is illustrated in Figure 2-22.

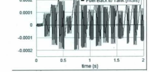

Figure 2-22 97% Model Regulator Output Fuel Flow Transient Response

2.5 Model Selection

In many cases the 98% model will be a good choice for modeling a typical fuel injection system. The pressure and flow transients (Figure 2-19 and Figure 2-20) match reasonably well those of the complete model (Figure 2-15 and Figure 2-16).

The benefits to using the 98% model over the complete model include:

- Less complexity (less elements)
- Improved computational efficiency
    - 19.4% less computations required for simulation
    - 46.6% less computation/simulation time

The 98% model is shown in Figure 2-23.

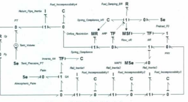

Figure 2-23 98% Model

2.6 Conclusion

The reduced model presented in this chapter was intended to provide an accurate representation of the complete system in terms of both transient and steady state responses.

However, the best selection of model to use will be based on the intended application for which it is to be applied. For example, if the intention is to study, in detail, the transient response, perhaps the complete model would be necessary in order to maintain the initial 4.7 kHz harmonic that was lost in the reduction process. Alternatively, if the study is focused on the steady state response of the system, the model could most likely undergo even further reduction than that presented in this chapter.

Beyond the consideration of model activity, other elements may be retained if they are of particular interest. For example, the fuel injector needle valves could be retained if the fuel injection pattern was part of the intended study.

Regardless, this chapter outlines the means by which one can reduce the complexity of a fuel delivery model, while still retaining the desired characteristics. Beyond reducing the computational complexity, the submodels of the system could also be imploded into iconic sections for easier analysis, as illustrated in Appendix D. A model with the proper degree of abstraction can be extremely useful as a design tool since it allows the engineer to focus on the elements of the system that have the greatest influence on performance.

Chapter 3 Pedal to Pavement: An Energy-Based Proper Vehicle Model

3.1 Introduction

Partial and complete vehicle models are an essential element of the design process within the automotive industry. Due to the prevalence of model-based design in this industry, a proper model of a complete vehicle can improve the efficiency of, at least, one stage of the design cycle.

Bond graphs are an efficient way of describing multiport systems in that the connections (bonds) between system elements have both an effort and a flow whose product is the power of the bond [7]. Moreover, bond graphs allow for the seamless interconnection of systems across energy domains (hydraulics, rotational mechanics, translational mechanics, electrodynamics, etc). Therefore, bond graphs are used as the preferred means of modeling presented in this chapter. For more details on bond graphs refer to [7].

In order for a complete vehicle model to suitably describe all significant system dynamics generated from pressing on the gas pedal to the resulting vehicle translation, it should suitably describe each of the major vehicle systems:

1. Fuel Delivery System
2. Air Induction System

3. Powertrain

4. Suspension

These systems are illustrated in the vehicle system cutaway in Figure 3-1, and are described in detail in the following sections.

Figure 3-1 Vehicle Cutaway (courtesy of CanadianDriver Communications Inc.)

3.2 Model Construction

3.2.1 Fuel Delivery System

The fuel delivery system pumps fuel from the fuel tank to the engine bay where it is atomized and sprayed by the fuel injectors. The model construction, reduction, and simulation of the fuel delivery system were detailed by the authors in [23].

3.2.2 Air Induction System

The air induction system measures and controls the air flow from the atmosphere to the engine cylinders.

3.2.2.1 Throttle Body

The throttle body allows air to pass from the atmosphere into the intake manifold. Its basis is a throttle (butterfly) valve which controls the amount of air allowed to enter. The mass airflow through the throttle body, $\dot{m}_{TB}$, can be expressed as choked flow through a converging nozzle, as given by (3-1) [24].

$$\dot{m}_{TB} = \begin{cases} \frac{C_D A_{TB} P_a}{\sqrt{R_{air} T_a}} \left(\frac{P_{man}}{P_a}\right)^{\frac{1}{\gamma}} \sqrt{\frac{2\gamma}{\gamma - 1}\left[1 - \left(\frac{P_{man}}{P_a}\right)^{\frac{\gamma-1}{\gamma}}\right]}, & \frac{P_{man}}{P_a} < P_c \\ \frac{C_D A_{TB} P_a}{\sqrt{R_{air} T_a}} \gamma^{\frac{1}{2}} \left(\frac{2}{\gamma + 1}\right)^{\frac{\gamma+1}{2(\gamma-1)}}, & \text{otherwise} \end{cases} \tag{3-1}$$

Where, C_D is the discharge coefficient of the throttle valve, A_{TB} is the effective area through which air may flow, P_a and T_a are the ambient pressure and temperature respectively, R_{air} and γ are the gas constant and adiabatic index specific to dry air respectively, P_{man} is the manifold pressure, and P_c is the critical pressure, above which the flow is choked.

The effective area, A_{TB}, can be approximated as the area of two circle segments created by the projection of the throttle valve onto the cross-section of the throttle body. This area is given by (3-2).

$$A_{TB} = \frac{D^2}{2}\left[\cos^{-1}\left\{\frac{\cos(\alpha + \alpha_c)}{\cos\alpha_c}\right\} - \frac{\cos(\alpha + \alpha_c)}{\cos\alpha_c}\sqrt{1 - \left[\frac{\cos(\alpha + \alpha_c)}{\cos\alpha_c}\right]^2}\right] \tag{3-2}$$

Where, D is the throttle body diameter, α is the variable angle by which the throttle is opened, and α_c is the throttle angle when it is fully closed. These parameters are illustrated in Figure 3-2.

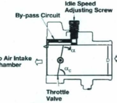

Figure 3-2 Throttle Body Side View (based on image courtesy of Toyota Motor Sales)

The bond graph form of the throttle body submodel is illustrated in Figure 3-3.

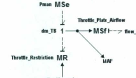

Figure 3-3 Throttle Body Submodel

3.2.2.2 Intake Manifold

The intake manifold distributes the delivered air through its runners to the engine cylinders. The manifold pressure, which directly affects most subsystems in the fuel delivery and air inductions system, is given by the ideal gas law, (3-3).

$$P_{man} = \left(m_{TB} - \sum m_{c,i}\right) \frac{R_{air} T_{man}}{V_{man}} \tag{3-3}$$

Where, $m_{c,i}$ is the air mass entering cylinder i, T_{man} and V_{man} are the temperature and volume of the manifold respectively.

This relationship, for a 4-cylinder engine, is given in bond graph form in Figure 3-4.

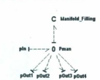

Figure 3-4 Intake Manifold Submodel

3.2.2.3 Cylinders

During the *intake stroke*, the intake valve is open and the cylinder in question is filled with the air-fuel mixture provided by the intake manifold runner and fuel injector. The mass airflow into a given cylinder, $\dot{m}_c$, is given by (3-4).

$$\dot{m}_c = \frac{P_{man}}{R_{air} T_{man}} \left(\frac{V_d}{2n_c}\right)\left(\frac{\omega_c}{2\pi}\right) \tag{3-4}$$

Where, V_d is the total engine displacement, n_c is the number of cylinders, and ω_c is the angular speed of the crankshaft.

Furthermore, during the *power stroke*, the air-fuel mixture undergoes combustion, whereby its mass is converted into energy, E_c, as given by (3-5).

$$E_c = \left(\frac{\dot{m}_c}{\omega_c}\right) \mathrm{H_u \eta_i} \tag{3-5}$$

Where, H_u is the heating value of the fuel and η_i is the indicated efficiency, given by the experimental equation, (3-6) [14].

$$\eta_i = 0.558(1 - 2.092\omega_c^{-0.36}) - 0.015 \tag{3-6}$$

These dynamics are represented as bond graphs in Figure 3-5.

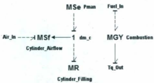

Figure 3-5 Cylinder Submodel

3.2.3 Powertrain

The powertrain consists of the system components that convert the energy from combustion into kinetic energy (i.e. movement).

3.2.3.1 Crankshaft

The crankshaft is driven by each piston during the *power stroke*, which effectively converts the combustion energy into a torque, τ_{in}. The crankshaft speed, ω_c, directly affects the fuel delivery and air induction systems, while the effective torque provided by the crankshaft, τ_{out}, affects the rest of the powertrain. These quantities are related via (3-7).

$$\omega_c = \frac{1}{I_{eff}} \int (\tau_{in} - \tau_f - \tau_{out})\, dt \tag{3-7}$$

Where, I_{eff} is the effective inertia as seen by the crankshaft and τ_f is the loss due to friction, which encompasses pumping losses during intake and exhaust strokes, rubbing friction between adjacent engine components, and losses associated with driving essential engine accessories. Furthermore, I_{eff} is given by (3-8), τ_f is calculated using the friction correlation, (3-9), adapted from [24], and τ_{out} is approximated as a parabola with a peak at the max indicated torque, τ_{max}, and passes through the max indicated power, P_{max}, at the indicated crankshaft speeds (ω_τ and ω_P), as shown in (3-10).

$$I_{eff} = I_e + I_t + \frac{I_d + (4m_w + m_v + m_p)(r_w/R_{FD})^2}{R_G^2} \tag{3-8}$$

$$\tau_f = \frac{V_d}{4\pi}(0.456\omega_c^2 + 143.24\omega_c + 9.7 \times 10^4) \tag{3-9}$$

$$\tau_{out} = \tau_{max} - \left(\tau_{max} - \frac{P_{max}}{\omega_P}\right)\left(\frac{\omega_c - \omega_\tau}{\omega_P - \omega_\tau}\right)^2 \tag{3-10}$$

Where, I_e, I_t, and I_d are the engine, transmission, and driveshaft inertias respectively, m_w, m_v, and m_p are the wheel, vehicle, and passenger(s) masses respectively, r_w is the wheel radius, R_{FD} and R_G are the final drive and (active) gear ratios respectively (described in the following sections).

The crankshaft dynamics are given in bond graph form in Figure 3-6.

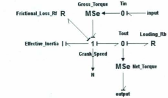

Figure 3-6 Crankshaft Submodel

3.2.3.2 Gearbox

The output torque from the crankshaft is applied to the input shaft of the gearbox. It contains a planetary gear / sun gear assembly which provide multiple discrete (for traditional transmissions) forward gear ratios, R_G, and a reverse gear ratio. Low gears are used to generate the higher torque required for getting the vehicle up to speed [25] while high (and overdrive) gears are used to improve efficiency at high speeds.

Gear selection is executed via a signal from the vehicle's Powertrain Control Module (PCM) or standalone Transmission Control Unit (TCU). The PCM/TCU uses data from the vehicle speed sensor and throttle position sensor as indices in a 2D lookup table or *shift schedule*, to determine in which gear the gearbox should be.

Furthermore, the input and output shafts of the gearbox have an associated stiffness and damping which affects their rotation.

The gearbox submodel is illustrated in bond graph form in Figure 3-7.

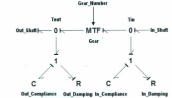

Figure 3-7 Gearbox Submodel

3.2.3.3 Differential

The differential takes the transverse rotation of the gearbox output shaft and converts it to longitudinal rotation, in order to drive the wheels.

Another torque multiplication is applied via the final drive ratio, R_{FD}, before being applied (in equal amounts) to the driven wheels. Moreover, the wheels are permitted to rotate at different speeds to facilitate maneuvering [26].

The differential submodel is shown in bond graph form in Figure 3-8.

Figure 3-8 Differential Submodel

3.2.3.4 Wheels

The torque applied to the wheel by the differential, τ_w, is converted to a tractive force, F_T, which causes the vehicle to move. This relationship is given by (3-11).

$$F_T = \frac{\tau_w}{r_w} - F_L \tag{3-11}$$

Where, F_L is the loss due to rolling resistance. For the non-driven wheels, $\tau_w = 0$.

The wheel submodel is shown in bond graph form in Figure 3-9.

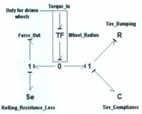

Figure 3-9 Wheel Submodel

The resulting speed of the vehicle, v_v, can be determined by accumulating the forces acting upon the vehicle, and applying Newton's 2nd law, as given by (3-12).

$$v_v = \int \frac{\sum F_{T,i} - F_D - F_R}{m_v + m_p} dt \tag{3-12}$$

Where, F_D is the aerodynamic drag given by (3-13) [27] and F_R is the loading due to the road profile, given by (3-14).

$$F_D = \frac{1}{2} C_d \rho_{air} A_F v_v^2 \tag{3-13}$$

$$F_R = (m_v + m_p)g \sin\theta_R \tag{3-14}$$

Where, C_d is drag coefficient, ρ_{air} is the density of air, A_F is the vehicle frontal area, g is the acceleration due to gravity, and θ_R is the angle of inclination of the road.

3.2.4 Suspension

The function of a vehicle's suspension is to either provide suitable ride quality (e.g. by smoothing out bumps in the road), improved handling (e.g. tight cornering), or some compromise between the two.

3.2.4.1 Struts

Typically, struts consists of a coil spring to support the vehicle's weight, a strut housing to provide rigid structural support for the assembly, and a damping unit within the strut housing to control spring and suspension movement [28].

The bond graph representation of a strut is given in Figure 3-10.

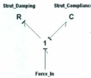

Figure 3-10 Strut Submodel

Furthermore, if the vehicle utilizes shock absorbers instead of struts, on two or four of the corners of the vehicle, the bond graph model is the same, but the element values are different.

3.2.4.2 Tires

The tires also act as a stiff spring to support the weight of the vehicle.

The bond graph representation of each tire was given previously with the wheel submodel in Figure 3-9.

3.2.5 Submodel Interconnection

Due to the nature of bond graphs, the submodels can be easily interconnected to form the complete vehicle model.

3.3 Model Reduction

By utilizing a method that quantizes the contribution of each element, one can make an informed decision regarding which elements to retain and which to eliminate from a proper model. A proper model has minimal complexity, physically meaningful parameters, and accurately predicts dynamic system responses [4].

The Model Order Reduction Algorithm (MORA) uses activity, A_i, to quantize the contribution of a given element. Activity is "absolute energy" and, for a given element i, is calculated by (3-15) [4].

$$A_i = \int |P_i(t)|\, dt \tag{3-15}$$

Where, P_i is the instantaneous power of element i.

Each element is assigned a non-dimensional activity index, AI_i, which is its fraction of the total system activity. For a given element i of k elements, its activity index is calculated using (3-16) [4].

$$AI_i = \frac{A_i}{A_{Total}} = \frac{\int |P_i(t)|\, dt}{\sum_{i=1}^{k} \{\int |P_i(t)|\, dt\}} \tag{3-16}$$

Activity indices are then sorted and elements eliminated from the lower end until the minimum number of elements required to satisfactorily reproduce the responses of the complete model is achieved.

3.3.1 Element Elimination

In order to properly exercise the model, three 30-second simulation profiles were executed to acquire activity data:

1. Full throttle, flat road
2. 50% throttle, 15° inclined road
3. Variable throttle, 1° inclined road

In the following discussion, *Profile 3* (variable throttle) will be used for illustration, and its activity analysis is given in Appendix E.

By following the MORA, the following 43 of 65 submodel elements can be eliminated and still produce simulation results with reasonable agreement to the complete model:

3.3.1.1 Fuel Delivery System

- Pressure Regulator submodel
- Return and Fuel Pipe submodels
- Resistances, inertias, and compressibilities (Fuel Rail submodel)
- Leakage coefficient (Fuel Pump submodel)

3.3.1.2 Powertrain

- Damping and compliances (Gearbox submodel)
- Driveshaft, engine inertias, and wheel mass (Crankshaft submodel)

3.3.1.3 Suspension

- Damping and compliances (Wheel and Strut submodels)

If the MORA were to be strictly followed, the following would also have been eliminated:

- Needle valves (Injector submodels)
- Spring compliance (Pulsation Damper submodel)
- Manifold filling (Intake Manifold submodel)
- Cylinder filling (Cylinder submodels)

However, these submodel elements were retained because of their physical meaningfulness. While the elements may not be active in terms of their power or energy, they provide important signals to be used by other parts of the model.

The injector needle valves provide the discretized fuel packets which provide the energy for the powertrain (via combustion).

The pulsation damper spring compliance (or stiffness) determines the fuel rail pressure used for fuel injection.

The manifold and cylinder filling determines (in conjunction with the throttle body submodel) the manifold pressure used throughout the fuel delivery and air induction systems.

3.3.2 Reduced Model Validation

Model outputs for the application presented in this chapter are manifold pressure, P_{man}, crank speed, ω_c, and vehicle speed, v_v. The simulation results for these quantities for the complete and reduced models are compared in Figure 3-11 to Figure 3-13.

One can see that the simulation results from reduced model follow the complete model relatively well. Based on the given application, the agreement is considered adequate.

The complexity of the complete model, shown in Appendix F, and reduced model, shown in Appendix G, can also be easily compared by observing the model structure.

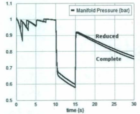

Figure 3-11 Manifold Pressure Curves for Complete and Reduced Models

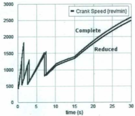

Figure 3-12 Crank Speed Curves for Complete and Reduced Models

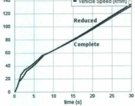

Figure 3-13 Vehicle Speed Curves for Complete and Reduced Models

3.4 Conclusion

The reduced model presented in this chapter consists of the 22 most active of 65 elements, yet still provides simulation results of adequate agreement to the complete model. By eliminating 43 elements, model calculations were reduced from an average of 3 041 653 to 437 960 (about 86%) for 30 seconds of simulation. Furthermore, simulation time was reduced from an average of 142 seconds to 12 seconds (about 92%). It is also important to note that the reduced model still retained over 98% of the original system activity.

Moreover, any further attempt to eliminate system elements resulted in large simulation deviations from those of the complete model. These deviations were most prominent when they caused the automatic transmission to change gears at a time other than that of the complete model.

The definition of "adequate agreement" obviously depends on the application. The application presented in this chapter considers throttle angle and road profile to be the inputs and manifold pressure, crank speed, and vehicle speed to be the outputs. However, if one was interested in studying ride quality, throttle angle and road profile might still be the inputs, but the most important output may be strut displacement, for example. Therefore, more elements may need to be retained (the reduced model presented eliminated the entire suspension system) or *different* elements may be able to be eliminated and still provide results for that application's "adequate agreement".

The implication of the material presented in this chapter is reflected in improving the efficiency of model-based design by reducing simulation time and model complexity. Furthermore, such models as the one presented can be used to predict vehicle characteristics such as fuel economy and performance (e.g. 0-60 and quarter-mile times).

Beyond reducing the computational complexity, the submodels of the system could also be imploded into iconic sections for easier analysis, as illustrated in Appendix H.

validation, this method would not suffice for validation of complete vehicle models, due to ignoring the effects of the driveline as well as external factors.

Chassis dynamometers would be more typical for validation of complete vehicle models. These dynamometers use rollers to characterize the vehicle output at the wheels. However, this method still does not include external factors such as the road profile or aerodynamic drag.

4.1.2 Real-World Model Validation

This chapter discusses a method of real-world vehicle model validation that logs vehicle and engine data as a vehicle is being driven on real roads, using a combination of OBD-II (On-Board Diagnostics, version II) and GPS (Global Positioning System) technologies.

The model used for validation, using the methodology to be discussed, is described in the following sections.

4.2 Proper Vehicle Model

A complete vehicle model was presented in [29] using bond graphs – a graphical method of modeling, similar in structure to a chemical bond, with a construction that is independent of energy domain. For more details on bond graphs refer to [7].

Furthermore, [29] reduces the complete model, using MORA (Model Order Reduction Algorithm), to a proper model. A *proper model* is one that has minimal complexity, physically meaningful parameters, and accurately predicts dynamic system responses [4].

This proper model is validated using the methods discussed in this chapter. For completeness, the model is described in the following subsections.

4.2.1 Fuel Delivery System

The modeling of the fuel delivery system was shown in extensive detail in [30]. After the model reduction in [29], the pulsation damper and fuel injector subsystems were retained. These subsystems are described in the sections below and are illustrated in Appendix I.

4.2.1.1 Pulsation Damper

The dynamics of the pulsation damper (i.e. accumulator) bolt-diaphragm assembly are given by (4-1).

$$P_R - P_a = \frac{k_A}{A_A} \int Q_A \, dt \tag{4-1}$$

Where, P_R and P_a are the fuel rail and ambient pressures, respectively, k_A is the stiffness of the bolt-diaphragm assembly (the inverse of the compliance, C_A), A_A is the cross-sectional area of the pulsation damper, and Q_A is the fuel flow into the pulsation damper.

This relationship is represented in bond graph form as illustrated in Figure 4-1.

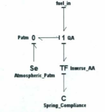

Figure 4-1 Pulsation Damper Submodel

4.2.1.2 Fuel Injectors

The mass flow rate of fuel injected by the fuel injector needle valves, $\dot{m}_{inj}$, is given by (4-2).

$$\dot{m}_{inj} = \begin{cases} C_d A_V \sqrt{2\rho_f (P_R - P_{man})}, & \text{ON} \\ 0, & \text{OFF} \end{cases} \tag{4-2}$$

Where, C_d is the internal discharge coefficient of the injector valve, A_v is the cross-sectional area of the injector valve, ρ_f is the density of fuel, and P_{man} is the manifold pressure.

A fuel injector is represented in bond graph form as illustrated in Figure 4-2.

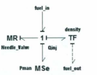

Figure 4-2 Fuel Injector Submodel

4.2.2 Air Induction System

The complete air induction system was retained after the model reduction described in [29], including the throttle body, intake manifold, and cylinder subsystems. These subsystems are described in the sections below.

4.2.2.1 Throttle Body

The mass airflow past the throttle (butterfly) valve, $\dot{m}_{TB}$, is given by (4-3) [24].

$$\dot{m}_{TB} = \begin{cases} \dfrac{C_D A_{TB} P_a}{\sqrt{R_{air} T_a}} \left(\dfrac{P_{man}}{P_a}\right)^{\frac{1}{\gamma}} \sqrt{\dfrac{2\gamma}{\gamma - 1}\left[1 - \left(\dfrac{P_{man}}{P_a}\right)^{\frac{\gamma-1}{\gamma}}\right]}, & \dfrac{P_{man}}{P_a} < P_c \\ \dfrac{C_D A_{TB} P_a}{\sqrt{R_{air} T_a}} \gamma^{\frac{1}{2}} \left(\dfrac{2}{\gamma + 1}\right)^{\frac{\gamma+1}{2(\gamma-1)}}, & \text{otherwise} \end{cases} \tag{4-3}$$

Where, C_D is the discharge coefficient of the throttle valve, A_{TB} is the effective area through which air may flow, T_a is the ambient temperature, R_{air} and γ are the gas constant and adiabatic index specific to dry air respectively, and P_c is the critical pressure, above which the flow is choked.

Furthermore the effective area, A_{TB}, is given by (4-4).

$$A_{TB} = \frac{D^2}{2}\left[\cos^{-1}\left\{\frac{\cos(\alpha+\alpha_c)}{\cos\alpha_c}\right\} - \frac{\cos(\alpha+\alpha_c)}{\cos\alpha_c}\sqrt{1-\left[\frac{\cos(\alpha+\alpha_c)}{\cos\alpha_c}\right]^2}\right] \tag{4-4}$$

Where, D is the throttle body diameter, α is the variable angle by which the throttle is opened, and α_c is the throttle angle when it is fully closed. These parameters are illustrated in Figure 4-3.

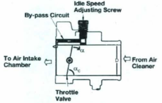

Figure 4-3 Throttle Body Side View (based on image courtesy of Toyota Motor Sales)

The bond graph form of the throttle body submodel is illustrated in Figure 4-4.

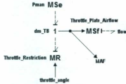

Figure 4-4 Throttle Body Submodel

4.2.2.2 Intake Manifold

The intake manifold pressure formulated using the ideal gas law, (4-5).

$$P_{man} = \left(m_{TB} - \sum m_{c,i}\right) \frac{R_{air} T_{man}}{V_{man}} \tag{4-5}$$

Where, $m_{c,i}$ is the air mass entering cylinder i, T_{man} and V_{man} are the temperature and volume of the manifold respectively.

This relationship, for a 4-cylinder engine, is given in bond graph form in Figure 4-5.

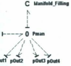

Figure 4-5 Intake Manifold Submodel

4.2.2.3 Cylinders

The mass airflow into a given cylinder, $\dot{m}_c$, is given by (4-6).

$$\dot{m}_c = \frac{P_{man}}{R_{air} T_{man}} \left(\frac{V_d}{2n_c}\right) \left(\frac{\omega_c}{2\pi}\right) \tag{4-6}$$

Where, V_d is the total engine displacement, n_c is the number of cylinders, and ω_c is the angular speed of the crankshaft.

During combustion the mass is converted into energy, E_c, as given by (4-7).

$$E_c = \left(\frac{\dot{m}_c}{\omega_c}\right) H_u \eta_i \tag{4-7}$$

Where, H_u is the heating value of the fuel and η_i is the indicated efficiency, given by the experimental equation, (4-8) [14].

$$\eta_i = 0.558(1 - 2.092\omega_c^{-0.36}) - 0.015 \tag{4-8}$$

These dynamics are represented as bond graphs in Figure 4-6.

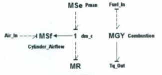

Figure 4-6 Cylinder Submodel

4.2.3 Powertrain

The reduced subsystems of the powertrain (crankshaft, gearbox, differential, and wheels) are described in the sections below.

4.2.3.1 Crankshaft

The torque, τ_{in}, resulting from combustion is converted to the crankshaft speed, as described by (4-9).

$$\omega_c = \frac{1}{I_{eff}} \int (\tau_{in} - \tau_f - \tau_{out})\, dt \tag{4-9}$$

Where, I_{eff} is the effective inertia as seen by the crankshaft and τ_f is the loss due to friction, and τ_{out} is the effective torque output.

Furthermore, I_{eff} is given by (4-10), τ_f is calculated using the friction correlation (4-11), adapted from [24], and τ_{out} is approximated as a parabola with a peak at the max indicated torque, τ_{max}, and passes through the max indicated power, P_{max}, at the indicated crankshaft speeds (ω_τ and ω_P), as shown in (4-12).

$$I_{eff} = I_t + (m_v + m_p)\left(\frac{r_w}{R_G R_{FD}}\right)^2 \tag{4-10}$$

$$\tau_f = \frac{V_d}{4\pi}(0.456\omega_c^2 + 143.24\omega_c + 9.7 \times 10^4) \tag{4-11}$$

$$\tau_{out} = \tau_{max} - \left(\tau_{max} - \frac{P_{max}}{\omega_P}\right)\left(\frac{\omega_c - \omega_\tau}{\omega_P - \omega_\tau}\right)^2 \tag{4-12}$$

Where, I_t is the transmission inertia, m_v and m_p are the vehicle, and passenger(s) masses respectively, r_w is the wheel radius; R_{FD} and R_G are the final drive and (active) gear ratios.

The crankshaft dynamics are given in bond graph form in Figure 4-7.

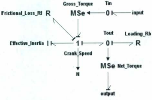

Figure 4-7 Crankshaft Submodel

4.2.3.2 Gearbox

The reduced submodel of the gearbox contains only a modulated transformer which converts the torque from the crankshaft to the differential based on the gear ratio of the selected gear.

4.2.3.3 Differential

The differential introduces another torque transformation based on the final drive ratio and distributes the resulting torque to the wheels.

4.2.3.4 Wheels

The torque applied to each wheel by the differential, τ_w, is converted to a tractive force, F_T, as given by (4-13).

$$F_T = \frac{\tau_w}{r_w} - F_L \tag{4-13}$$

Where, F_L is the loss due to rolling resistance. For the non-driven wheels, $\tau_w = 0$.

The wheel submodel is shown in bond graph form in Figure 4-8.

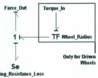

Figure 4-8 Wheel Submodel

The resulting speed of the vehicle, v_v, is given by (4-14).

$$v_v = \int \frac{\sum F_{T,i} - F_D - F_R}{m_v + m_p} dt \tag{4-14}$$

Where, F_D is the aerodynamic drag given by (4-15) [27] and F_R is the loading due to the road profile, given by (4-16).

$$F_D = \frac{1}{2} C_d \rho_{air} A_F v_v^2 \tag{4-15}$$

$$F_R = (m_v + m_p) g \sin\theta_R \tag{4-16}$$

Where, C_d is drag coefficient, ρ_{air} is the density of air, A_F is the vehicle frontal area, g is the acceleration due to gravity, and θ_R is the angle of inclination of the road.

4.2.4 Suspension

The suspension submodels were completely eliminated by the model reduction of [29].

4.3 Model Additions

Because the model described in the previous sections was intended to describe a vehicle under throttle and cruising (as would be validated using a dynamometer), some practical considerations need to be taken into account for on-road modeling.

4.3.1 Idling

The above model used a constantly open or modulated throttle to illustrate its effect. However, when a driver does not have the gas pedal depressed, the throttle (butterfly) valve that regulates airflow into the intake manifold is completely closed.

If the only source of air is shut off, the engine will not be able to perform proper combustion and will stall. Therefore, consideration must be given to the "idle bypass circuit" which allows air to flow when the throttle is closed (the amount of which is determined by the idle speed adjustment screw). This was shown in Figure 4-3.

Taking this bypass airflow, $\dot{m}_B$, into account, the original expression for mass airflow past the throttle valve, $\dot{m}_{TB}$, given by (4-3), would now be expressed as $\dot{m}'_{TB}$, given by (4-17).

$$\dot{m}'_{TB} = \dot{m}_{TB} + \dot{m}_B \tag{4-17}$$

4.3.2 Braking

The original model considered a cruising vehicle – one that was either accelerating or decelerating solely based on system losses and external forces.

However, under normal driving conditions, it is impractical to expect a driver to coast to every stop. Therefore, consideration must be given to the braking pattern (the duration and brake pedal displacement) resulting in a braking force, F_B, given by (4-18).

$$F_B = \left(\frac{r_W}{r_R}\right) F_T \tag{4-18}$$

Where, r_R is the radius of the rotor.

Taking this braking force into account, the original expression for tractive force, F_T, given by (4-13), would now be expressed as F'_T, given by (4-19).

$$F'_T = F_T - F_B \tag{4-19}$$

The resulting bond graph for the wheel submodel is shown in Figure 4-9.

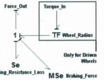

Figure 4-9 Wheel Submodel with Braking

The additions outlined above are reflected in the updated model illustrated in Appendix J.

4.4 Model Inputs

The main variable inputs of interest to this model are the road profile, throttle position, and braking pattern. Furthermore, there are a number of parameters (values that may vary between vehicles or between datasets, but remain constant for a given dataset) that contribute to the performance of the model. These inputs are described in the sections below.

4.4.1 Published Parameters

The parameters given in Table 4-1, used as model inputs, are quantized by published or publicly available data such as marketing brochures, datasheets, or mechanic manuals.

Table 4-1 Published Parameters

Parameter	Symbol	Units
Engine Displacement	V_d	L
# of Cylinders	n_c	-
Engine Power [a]	P_{max}	hp (or kW)
Engine Torque [a]	τ_{max}	ft-lbs (or N-m)
Pump Flow Rate	Q_{PT}	lph (or gph)
Injector Flow Rate	Q_{inj}	lbs/h (or cc/min)
# of Transmission Gears	n_G	-
Transmission Gear Ratios	R_G	-
Final Drive Ratio	R_{FD}	-
Tire Width	w_t	mm
Tire Profile	p_t	%
Tire Diameter	d_t	in
Vehicle mass	m_v	lbs (or kg)
Weight Distribution	D_w	-
Frontal Area	A_F	m^2 (or ft^2)
Aerodynamic Drag Coefficient	C_d	-

[a] Engine power and torque are also provided at their respective crankshaft speeds, ω_P and ω_τ, respectively.

4.4.2 Measured Parameters

The parameters given in Table 4-2, used as model inputs, are quantized through manual measurement.

Table 4-2 Measured Parameters

Parameter	Symbol	Units
Ambient Temperature [b]	T_a	°C (or °F)
Ambient Pressure [b]	P_a	kPa (or bar or atm)
Throttle Body Diameter	D	mm
Intake Manifold Volume [c]	V_{man}	m^3
Rotor radius	r_R	cm (or in)

[b] Ambient conditions can be measured using a digital weather station or similar system of transducers.
[c] Intake manifold volume can be considered the sum of its parts – the plenum can be considered, in most cases, to be a box and the runners (one per cylinder) can be considered as cylinders.

4.4.3 Estimated Parameters

The parameters given in Table 4-3, used as model inputs, are quantized based on estimations.

Table 4-3 Estimated Parameters

Parameter	Symbol	Units
Transmission Inertia [d]	I_t	kg-m^2
Coefficient of Rolling Resistance [e]	C_R	-

[d] Based on the literature (such as [31]), the inertia of the rotating components of the transmission is on the order of 0.4 kg-m^2.
[e] According to [24], the coefficient of rolling resistance is in the range 0.012-0.015

4.4.4 Logged Parameters

The parameters given in Table 4-4, used as model inputs, are quantized through data obtained via OBD-II. The method of data logging via OBD-II is described later in this chapter.

Table 4-4 Logged Parameters

Parameter	Symbol	Units
Equivalence Ratio	φ	-
Intake Manifold Temperature [f]	T_{man}	°C
Closed Throttle Angle	α_c	deg (or rad)
Idle Crankshaft Speed	ω_{idle}	rad/s
Transmission Shift Schedule [g]	-	-

[f] The temperature remains reasonably constant throughout any given dataset, therefore it can be considered a model parameter rather than a variable input.
[g] Assuming that the shift schedules are 2D lookup tables that output gear number based on throttle position and vehicle speed, one can regenerate the table by logging these indices and monitoring crankshaft speed for discontinuities.

4.4.5 Logged Variable Inputs

The variables given in Table 4-5, used as model inputs, are quantized dynamically through data obtained in real-time via GPS and OBD-II. These methods of data logging are described later in this chapter.

Table 4-5 Logged Variable Inputs

Parameter	Symbol	Units
Road Profile	θ_R	deg (or rad)
Throttle Position	α	deg (or rad)
Braking Pattern [h]	F_B	N

[h] The vehicle braking pattern is derived from analyzing the crankshaft and vehicle speed and fitting a percentage of the maximum braking force.

4.5 Model Outputs

The outputs of interest for this model are the intake manifold pressure, the crankshaft speed, and the vehicle speed. These outputs are described in the sections below.

4.5.1.1 Intake Manifold Pressure

The intake manifold pressure (in kPa) can be determined by requesting data from the intake manifold pressure sensor. This sensor is available typically in vehicles that meter fuel using the speed-density technique.

4.5.1.2 Crankshaft Speed

The crankshaft speed (in RPM) can be determined by requesting data from the crankshaft position sensor.

4.5.1.3 Vehicle Speed

Vehicle speed can be determined either by requesting data from the vehicle speed sensor (in km/h) or acquired using GPS (in knots). The former was used for this project.

4.6 Model Validation Test Setup

Multiple routes and different vehicles were used to generate a variety of scenarios in which to exercise the model and verify its versatility.

An example of a route used for one of the datasets is shown in Figure 4-10.

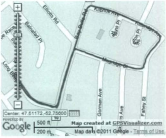

Figure 4-10 Example Route

Data was collected using two distinct vehicles – a 2004 Chevrolet Optra (a 1250kg, 2.0L compact sedan) and a 2003 Honda CR-V (a 1525kg, 2.4L sport utility vehicle).

The plots shown throughout this chapter illustrate the first 60 seconds of data for the given dataset to maintain figure clarity.

4.7 Data Logging Technology and Methodology

Two distinct data logging technologies are required to capture the real-time information necessary to properly exercise the model. The global positioning and diagnostic technologies used are described in the following sections.

4.7.1 Use of Global Position Data

The ability to generate a road profile is not possible solely using data available from OBD-II. Therefore, GPS was used to acquire altitude/elevation data.

Altitude is available directly via GPS by decoding the GGA (Global Positioning System Fix Data) sentence (10th word, in m). However, according to [32], this altitude can have an error up to ±400ft (122m) for many consumer GPS, due to arrangement of satellite configurations during fix determinations.

However, the SRTM (Shuttle Radar Topography Mission), which was launched by NASA (National Aeronautics and Space Administration) on February 11 2000, obtained elevation data on approximately 80% of Earth landmass with up to 4 sets of redundant mappings, according to [33]. Furthermore, [34] shows that the error in the altitude data collected by the SRTM is less than 5m for terrain profiles under 10°.

Therefore, using a web utility provided by *GPS Visualizer*, one can query the SRTM database for altitude data using a latitude-longitude pair decoded from an RMC (Recommended Minimum sentence C) NMEA (National Marine Electronics Association) sentence.

4.7.2 Global Position Data Logging and Analysis

Global positioning data was collected using a Canmore GT-730F USB GPS Receiver (based on the SkyTraq Venus 6 chipset).

TeraTerm was used to log and timestamp the GPS NMEA stream received via USB as shown in Figure 4-11. GPS data was updated every 1 second.

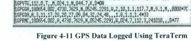

Figure 4-11 GPS Data Logged Using TeraTerm

A Perl script was written to extract the latitude and longitude data from the RMC NMEA sentences (as discussed above) contained in the log and parse them into a format to be used by *GPS Visualizer*. As an example, one of the altitude data sets returned by the SRTM database is shown in Figure 4-12.

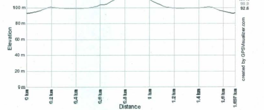

Figure 4-12 CR-V Altitude Data

The resulting altitudes in conjunction with timestamps and vehicle speeds (also parsed by the Perl script) were used to calculate the road profile (i.e. elevation), θ_R, using (4-20), which was used as a model input.

$$\theta_R = \tan^{-1}\left(\frac{\Delta h_i}{d_i}\right), \theta_R \in [-\pi, \pi] \tag{4-20}$$

Where, Δh_i is the difference in the current and previous altitudes (in m) and d_i is the distance traveled since the last sample (in m), given by the right Riemann sum in (4-21).

$$d_i = v_i \Delta t_i \tag{4-21}$$

Where, v_i is the current vehicle speed (in m/s) and Δt_i is the time since the last sample (in s).

Furthermore, the computed road profiles were smoothed using a moving average filter. The averaging filter uses local regression using weighted linear least squares and a 2nd degree polynomial model while assigning lower weight to outliers in the regression, as described by [35].

The road profiles used as inputs in the datasets described in this chapter are shown in Figure 4-13 and Figure 4-14.

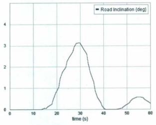

Figure 4-13 Optra Road Profile Input

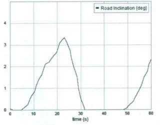

Figure 4-14 CR-V Road Profile Input

4.7.3 Use of Diagnostic Data

OBD-II is available on all North American cars and light trucks manufactured since 1996, and provides various metrics to describe the current state of a vehicle.

As per [36], *Service 01* of the OBD-II J1979 standard provides "Current Powertrain Diagnostic Data" which allows access to current emission-related data values. This provides a means by which to collect most of the necessary data for model inputs and validation of model outputs.

4.7.4 Diagnostic Data Logging and Analysis

OBD-II has nine variations of communication protocols (under ISO 15765-4, ISO 9141-2, ISO 14230-4, and SAE J1850). Therefore, a beta version of OSAPI™ (One Simple Application Programming Interface) shown in Figure 4-15, developed by Lemur Vehicle Monitors (a division of Root Four Imagination Inc), was used to handle OBD-II bus arbitration and interpretation, and the resulting vehicle data was re-transmitted via UART.

Figure 4-15 OSAPI™ by Lemur Vehicle Monitors

A custom external UART to USB module was developed to allow the UART data provided by OSAPI™ to be logged by a PC. TeraTerm was used as a terminal emulator to log (and timestamp) the data from the USB stream, as shown in Figure 4-16.

Figure 4-16 Diagnostic Data Logged Using TeraTerm

Due to timing limitations of the OBD-II protocols used in the test vehicles, and the number of variables being logged, each dataset was updated approximately every 1 second.

A Perl script was written to extract the data from the diagnostic log and parse into a format to be used by the model software (*20-Sim*).

The throttle positions used as inputs in the datasets described in this chapter are shown in Figure 4-17 and Figure 4-18.

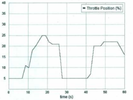

Figure 4-17 Optra Throttle Position Input

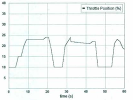

Figure 4-18 CR-V Throttle Position Input

The three model outputs of interest (manifold pressure, crankshaft speed, and vehicle speed) were also logged. The logged (OBD) values were plotted on the same axes as the values predicted by the model, as shown in Figure 4-19 to Figure 4-24.

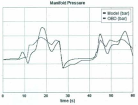

Figure 4-19 Optra Manifold Pressure Output

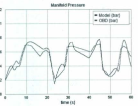

Figure 4-20 CR-V Manifold Pressure Output

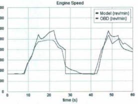

Figure 4-21 Optra Crankshaft Speed Output

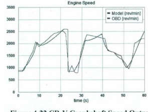

Figure 4-22 CR-V Crankshaft Speed Output

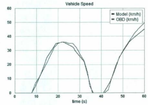

Figure 4-23 Optra Vehicle Speed Output

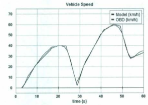

Figure 4-24 CR-V Vehicle Speed Output

4.8 Statistical Analysis

The plots presented above appear at first glance to be a reasonable approximation of the actual (OBD) data collected. In order to provide a means to quantify the fit of the model, multiple linear regression (using least squares) was performed on the data pairs.

The coefficients of determination (R^2) resulting from the regression analysis are given in Table 4-6.

Table 4-6 Coefficients of Determination (R^2)

Output	Optra	CR-V
Manifold Pressure	0.7154	0.8355
Crankshaft Speed	0.9001	0.9068
Vehicle Speed	0.9953	0.9951

It is unsurprising that the value of R^2 in each dataset increases in each row of Table 4-6 due to the fact that the sensitivity of each output decreases. An output that has a higher sensitivity may have more unpredictable behavior when comparing a modeled versus real-world response.

Manifold pressure will react quickly to any change in throttle position or fuel metering as it is directly proportional to the air mass entering the intake manifold and exiting into the cylinders.

Crankshaft speed is the result of the integration of the combustion resulting from the air-fuel mixture injected into the cylinders. This integration will act as a low-pass filter and will therefore be less sensitive to minor disturbances.

Similarly, vehicle speed is the result of the integration of forces acting on the vehicle. Comparatively, more inertia will be prevalent in vehicle speed than crankshaft speed, making it even less sensitive to minor disturbances.

While R^2 is not, in and of itself, enough to prove that a model is an accurate predictor, it is a factor in indicating "goodness of fit". When considered in conjunction with the facts that significantly different vehicles (i.e. significantly different model parameters) were used on different routes (i.e. different variable inputs) between datasets, one could make a fair conclusion that the model presented is an accurate predictor of the dynamics of a vehicle.

4.9 Conclusion

There are two points of significance raised in the preceding discussions of this chapter.

Firstly, it was shown that a complete vehicle model can be constructed and systematically reduced (via an algorithm such as MORA), while still providing accurate predictions consistent with real-world data. Furthermore, as discussed in [30], the reduced proper model still contained over 98% of the energy of the complete model, yet reduced model complexity by about 86% and simulation time by about 92%. Such a model can allow a designer to accurately predict vehicle performance in terms of fuel economy and emissions, as well as 0-60 and quarter mile times.

Secondly, it was shown that feasible methods are available to validate a vehicle model using real-time and real-world data, using a combination of GPS and OBD-II technologies. This illustrates that vehicle model validation need not be constricted to simulation comparisons or dynamometer testing that do not properly exercise a vehicle as it would typically be on actual driven roads.

Automotive engineers and designers using a model-based design approach should give careful consideration to the modeling and model validation techniques which they adopt.

Proper modeling can greatly reduce model complexity and simulation time, while maintaining important system dynamics. In terms of model validation, there is no sufficient substitute for actual road-driven real-world data with which to compare and analyze model predictions.

Chapter 5 Summary, Conclusions, and Recommendations

Chapter 2 through Chapter 4 describe in detail the process of proper modeling using bond graphs for, in this case, a road-ready vehicle model. From this, one can see that there are three distinct contributions to the field of automotive modeling:

1. Complete vehicle model construction
2. Model reduction to achieve a proper vehicle model
3. Vehicle model validation and validation techniques

These contributions and their potential implications are discussed in the following sections.

5.1 Complete Vehicle Model Construction

Chapter 2 and Chapter 3 detailed the construction of a complete vehicle model – one that contains the complete set of system dynamics and energy. Despite having elements from multiple domains (hydraulic, rotational mechanics, and translational mechanics), the construction, using bond graphs, allowed for the intuitive interconnection of the system submodels.

As the automotive industry moves more toward model-based design, such models and modeling techniques will be of significant interest to design engineers. A complete vehicle model allows an automotive engineer to study all dynamic system responses in great detail without the loss of resolution from improper model reduction. Furthermore, said engineer could also use a complete vehicle model as the reference point for a different proper model, depending on the response(s) of interest. For example, if the suspension dynamics were to be studied in detail, a different set of elements would potentially be eliminated, contrary to the elimination process discussed in Chapter 3.

5.2 Model Reduction to Achieve a Proper Vehicle Model

Chapter 2 went into extensive detail regarding the model reduction process, using the Model Order Reduction Algorithm (MORA), as it applies to automotive modeling. This process, in and of itself, gives a model-based designer an automotive reference point to use as a tool in creating efficient automotive models.

Chapter 3 implemented an extension of the model reduction process of Chapter 2 to develop a proper vehicle model – one that has minimal complexity, physically meaningful parameters, and accurately predicts dynamic system responses [4]. The significant implication of proper modeling to the model-based designer is in the ability to quantitatively eliminate elements that are not of interest to the specific application and thereby reduce the model complexity and simulation time.

Additionally, Chapter 4 extended the proper vehicle model developed in Chapter 3 to account for "road-readiness", allowing a model-based designer to exercise system responses as would be expected by a vehicle actually driven on the road. This empowers the designer with the ability to break away from the standard dyno-based validation methods, resulting in improved accuracy.

5.3 Vehicle Model Validation and Validation Techniques

As mentioned in the previous section, dyno-based model validation for automotive modeling has been the industry de-facto standard. However, dynamometers can be costly to purchase, maintain, and operate. Furthermore, they cannot necessarily account for certain external retarding/expediting factors, such as road profile and aerodynamic drag, which are required to properly validate a road-ready vehicle model.

Chapter 4 presented a method of on-road vehicle model validation using an inexpensive combination of GPS and OBD-II technologies. Because data is logged while a test vehicle is actually being driven, all external factors present in a real-world scenario are applied for comparison against the model predictions.

Moreover, this model validation technique was applied to the road-ready proper vehicle model described in Chapter 4 (adapted from Chapter 3). The model was shown to be accurate for two distinct vehicles (compact sedan and sport utility vehicle) on different geographical routes and thereby added credibility to the model, and the research as a whole, presented in this thesis.

5.4 Future Work and Potential Uses

The contributions of the research presented have their own inherent uses, as discussed in the previous sections. Furthermore, future work could be performed to expand on these uses – examples of potential uses are discussed in the following sections.

5.4.1 Complete/Proper Vehicle Model Simulink Blockset

There would be value in generating a custom automotive blockset for the more commonly used *Simulink* modeling software package. Because of the versatility of the vehicle model presented, a unified generic "complete vehicle" block could be built that accepts all the parameters outlined in Chapter 4 and allows the selection of desired output(s).

Moreover, proper vehicle model options could be provided which would optimize the internal structure of the unified generic block based on the selected application (e.g. loading/motion, suspension dynamics, system losses, etc).

Alternatively, each submodel discussed in Chapter 2 and Chapter 3 could be converted into a *Simulink* block. This would allow the designer to construct different vehicle configurations such as direct injection, inline fuel pumps, non-return fuel systems, rear-wheel drive, etc.

Each of the above blockset options (complete model and submodels) are natively supported by *20-Sim* for export to *Simulink*. The exportation as a modeling technique is discussed in [37].

5.4.2 Model Deployment to an Embedded Target

Deployment of the vehicle model to an embedded target, such as a Freescale MPC555 (common to the automotive industry) or similar processor, could allow for such a system to be used as a design tool or vehicle emulator for industrial development and testing or academic training.

The Mathworks *Real-Time Workshop Embedded Coder* facilitates the generation of ANSI/ISO C/C++ code from *Simulink* models to be programmed onto various processors, as discussed in [38]. By exporting the bond graph model from *20-Sim*, as discussed in the previous section, this method could be utilized for model deployment.

5.4.3 The Vehicle Model as an ECU Control Algorithm

Because the vehicle model presented accurately predicts vehicle outputs, based on the parameters and inputs described in Chapter 4, it could easily be converted into a control algorithm to *drive* these outputs. This lends the model to an ECU (Electronic Control Unit) design application.

AUTOSAR (AUTomotive Open System ARchitecture) is the standard architecture for ECU networks [39] that was developed primarily by its core members: BMW, Bosch, Continental, Daimler, Ford, GM, Peugeot/Citroën, Toyota, and VW. The AUTOSAR architecture is illustrated in Figure 5-1.

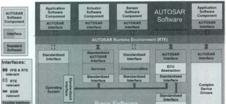

Figure 5-1 AUTOSAR Architecture [39]

Similar to the previous section, the Mathworks *Real-Time Workshop Embedded Coder* can generate AUTOSAR-compliant code [39] that would correspond to the "Software Components" blocks in the architecture diagram shown in Figure 5-1.

5.4.4 Integrated GPS/OBD Model Validation Tool

Expanding on the model validation techniques presented in Chapter 4, one could develop an integrated solution for vehicle model validation that handles the GPS logging, OBD logging, and data formatting, such that the final output log is ready for import into the model software as well as statistical analysis.

This would further facilitate the migration from dyno-based vehicle model validation that is (much) more costly and inaccurate.

5.4.5 Self-Validating Real-Time Model Platform

Expanding even further on the integrated validation solution proposed in the previous section, one can envision a fully-automated platform that is self-validating in real-time (as the data is logged).

Given a GPS module of sufficient altitude accuracy (or other transducer for measuring altitude/elevation or inclination), the variable inputs described in Chapter 4 could be logged, parsed, and fed directly into the model software package. The resulting outputs from the model software could then be compared using statistical tools against the outputs logged from the OBD-based validation platform. No intermediate manual post-processing steps would be required. Furthermore, this would allow for real-time tuning of the model parameters for applications that wish to fit the theoretical model to the real-world data.

5.5 Summary

One can certainly see the potential for such tools and techniques, resulting from the proper modeling process outlined in this thesis. As more automobile and OEM manufacturers move toward model-based design, a greater need to standardize such a process will arise.

The proper modeling process, proper vehicle model, and/or model validation techniques presented in this thesis may, by no means, be the solution to the arising need, but the illustration of the process as a whole shows the fundamental approach necessary for the automotive industry.

5.6 Bibliography and References

1. **Maplesoft.** Toyota and Maplesoft enter a multi-year partnership to produce new tools for knowledge-rich physical modeling. *Math Software for Engineers, Educators & Students.* [Online] November 8, 2007. [Cited: March 12, 2011.] http://www.maplesoft.com/company/publications/articles/view.aspx?SID=5476.

2. **The Mathworks.** GM Standardizes on Model-Based Design for Hybrid Powertrain Development. *User Story.* [News Article]. May 2009. 91714v00.

3. **Swoish, Jim.** Fusion Hybrid Energized. *dSPACE Magazine.* Paderborn, Germany : dSPACE GmbH, December 2010.

4. *Generating Proper Dynamic Models for Truck Mobility and Handling.* **Louca, Loucas S, et al.** December 29, 2003, International Journal of Heavy Vehicle Systems, pp. 1,4.

5. **Karnopp, Dean, Margolis, Donald L and Rosenberg, Ronald C.** *System Dynamics: A Unified Approach.* 2nd Edition. New York : Wiley-Interscience, 1990. 0471621714.

6. *Systematic Assessment of Rigid Internal Combustion Engine Dynamic Coupling.* **Rideout, Geoff, Stein, Jeffrey L and Louca, Loucas S.** 2, s.l. : ASME, 2008, Journal of Engineering for Gas Turbines and Power, Vol. 130, p. 2. 022804.

7. **Karnopp, Dean C, Margolis, Donald L and Rosenberg, Ronald C.** *System Dynamics - Modeling and Simulation of Mechatronic Systems.* 3rd. New York : Wiley-Interscience, 2000.

8. *Coverage Analysis for Model Based Design Tools.* **Aldrich, William.** 2001. TCS 2001.

9. *Modelling of Dynamic Responses of an Automotive Fuel Rail System, Part II: Entire System.* **Wu, S F, et al.** 5, s.l. : Academic Press, August 30, 2001, Journal of Sound and Vibration, Vol. 245, pp. 815-834. doi:10.1006/jsvi.2001.3597.

10. *Dynamic Modeling and Analysis of Automotive Multi-Port Electronic Fuel Delivery System.* **Yang, W C, et al.** March 1991, Journal of Dynamic Systems, Measurement, and Control, Vol. 113, pp. 147-148.

11. *Bond Graph Modeling and Simulation of a Full Car Model with Active Suspension.* **Adibi-asl, H and Rideout, D G.** Banff : IASTED, 2009. International Conference on Modelling and Simulation. 670-046.

12. *The Controller Output Observer: Estimation of Vehicle Tire Cornering and Normal Forces.* **Ozkan, Basar, Margolis, Donald and Pengov, Marco.** 6, s.l. : ASME, November 2008, Journal of Dynamic Systems, Measurement, and Control, Vol. 130. doi:10.1115/1.2957627.

13. *Mean Value Engine Modelling of Spark Ignition Engines.* **Hendricks, E and Sorenson, S C.** Detroit : SAE International, 1990. International Congress & Exposition. doi:10.4271/900616.

14. *A Generic Mean Value Engine Model for Spark Ignition Engines.* **Hendricks, Elbert, Engler, Donn and Fam, Marco.** Lyngby : Scandinavian Simulation Society, 2000. 41st Simulation Conference.

15. **Karmiggelt, Rob.** *Mean value modelling of a s.i. engine.* Department of Mechanical Engineering. Eindhoven : Eindhoven : Technische Universiteit Eindhoven, 1998. Stageverslag. - WFW 1998.041.

16. **Hedrick, J K, McMahon, D H and Swaropp, D.** *Vehicle Modeling and Control for Automated Highway Systems.* Institute of Transportation Studies, University of California, Berkeley. Berkeley : s.n., 1993. 1055-1425.

17. *Modeling of a hybrid electric vehicle powertrain test cell using bond graphs.* **Filippa, M, et al.** 3, s.l. : IEEE Vehicular Technology Society, May 23, 2005, IEEE Transactions on Vehicular Technology, Vol. 54, pp. 837-845. doi:10.1109/TVT.2005.847226.

18. **Merritt, Herbert E.** *Hydraulic Control Systems.* New York : John Wiley & Sons, Inc., 1967.

19. **Mathworks.** Resistive Tube. *MATLAB and Simulink for Technical Computing.* [Online] February 9, 2009. [Cited: May 16, 2009.] http://www.mathworks.com/access/helpdesk/help/toolbox/physmod/simscape/ref/resistivetube.html.

20. **Toyota Motor Sales, U.S.A., Inc.** Fuel Delivery & Injection Control. [book auth.] U.S.A., Inc. Toyota Motor Sales. *EFI Course Book.* 2001, pp. 8,15.

21. *On-Road Measurements of Emissions and Fuel Consumption of Gasoline Fuelled Light Duty Vehicles.* **Gonçalves, G A and Farias, T L.** Lisbon : s.n., 2005. Clean Air 2005 - Eight International Conference on Technologies and Combustion for a Clean Environment. p. 9.

22. **Browne, Greg.** *Design of Experiments to Determine Factors Contributing to Fuel Economy.* Faculty of Engineering, Memorial University. St. John's : Unpublished, 2008.

23. *An Energy-Based Proper Model of an Automotive Fuel Delivery System.* **Browne, Greg, Krouglicof, Nicholas and Rideout, Geoff.** Detroit : SAE International, 2010. SAE 2010 World Congress & Exhibition.

24. **Heywood, John B.** *Internal Combustion Engine Fundamentals.* New York : McGraw-Hill, Inc., 1988. p. 307.

25. **Toyota Motor Sales.** *Gear Selection and Function.* March 5, 2007.

26. **Driving Fast.** Differentials. *drivingfast.net.* [Online] [Cited: July 3, 2010.] http://www.drivingfast.net/technology/differentials.htm.

27. **Glenn Research Center, NASA.** The Drag Equation. *Glenn Research Center.* [Online] [Cited: July 8, 2010.] http://www.grc.nasa.gov/WWW/K-12/airplane/drageq.html.

28. **Monroe.** Struts. *Monroe Shocks & Struts.* [Online] 2008. [Cited: July 12, 2010.] http://www.monroe.com/support/tec_struts.asp.

29. *Pedal to Pavement: An Energy-Based Proper Vehicle Model.* **Browne, G and Krouglicof, N.** Manuscript sumbitted for publication.

30. **Browne, G, Krouglicof, N and G, Rideout.** An Energy-Based Proper Model of an Automotive Fuel Delivery System. [book auth.] SAE International. *Reliability and Robust Design in Automotive Engineering, 2010.* 2010.

31. *Design and Construction Aspects of a Zero Inertia CVT for Passenger Cars.* **Van Druten, R M, et al.** 1, s.l. : KSAE, June 12, 2000, International Journal of Automotive Technology, Vol. 1, pp. 42-47. 1229-9138.

32. **Garmin Ltd.** How accurate is the GPS elevation reading? *Garmin.* [Online] June 28, 2010. [Cited: September 12, 2010.] https://buy.garmin.com/support/searchSupport/case.faces?caseId={66f1b0a0-4cd6-11dc-4733-000000000000}.

33. **California Institute of Technology.** NASA Jet Propulsion Laboratory. *Data Coverage.* [Online] August 28, 2005. [Cited: September 12, 2010.] http://www2.jpl.nasa.gov/srtm/datacoverage.html.

34. *Accuracy assessment of the processed SRTM-based elevation data by CGIAR using field data from USA and Thailand and its relation to the terrain characteristics.* **Gorokhovich, Y and Voustianiouk, A.** 4, s.l. : ELSEVIER, October 30, 2006, Remote Sensing of Environment, Vol. 104, pp. 409-415. 0034-4257.

35. **Mathworks.** smooth. *Mathworks | Accelerating the pace of engineering and science.* [Online] 2007b. [Cited: October 19, 2010.] http://www.mathworks.com/help/toolbox/curvefit/smooth.html.

36. **SAE International.** *E/E Diagnostic Test Modes.* 2007. p. 24, Standard. J1979.

37. **Nohac, Karel and Nohacova, Lucie.** Possibilities of Computer Simulation in Power Engineering and Environmental Engineering. [ed.] Tarek Sobh. *Innovations and Advances in Computer Sciences and Engineering.* s.l. : Springer Science+Business Media, 2010, pp. 1-2.

38. *Prototyping of Control Algorithms in Matlab/Simulink.* **Grygiel, Rafal and Pacholczyk, Marcin.** Orlando : International Institute of Informatics and Systemics, 2010. Engineering and Technological Innovation: IMETI 2010.

39. *Development of AUTOSAR Software Components within Model-Based Design.* **Sandmann, Guido and Thompson, Richard.** Detroit : SAE International, 2008. SAE World Congress & Exhibition. 2008-01-0383.

5.7 Appendices

Appendix A Bond Graph Elements[6]

	SYMBOL	CONSTITUTIVE LAW (LINEAR)	CAUSALITY CONSTRAINTS
SOURCES			
Flow	$Sf \vdash\!\rightharpoonup$	$f = f(t)$	fixed flow out
Effort	$Se \rightharpoonup\!\mid$	$e = e(t)$	fixed effort out
ENERGETIC ELEMENTS			
Inertia	$\rightharpoonup\!\mid I$ $\vdash\!\rightharpoonup I$	$f = \frac{1}{I}\int e\,dt$ $e = I\frac{df}{dt}$	preferred integral
Capacitor	$\vdash\!\rightharpoonup C$ $\rightharpoonup\!\mid C$	$e = \frac{1}{C}\int f\,dt$ $f = C\frac{de}{dt}$	preferred integral
Resistor	$\vdash\!\rightharpoonup R$ $\rightharpoonup\!\mid R$	$e = Rf$ $f = \frac{1}{R}e$	none
2-PORT ELEMENTS			
Transformer	$\xrightharpoonup{1}\!\mid \underset{n}{TF} \xrightharpoonup{2}\!\mid$	$e_2 = n\,e_1$ $f_1 = n\,f_2$	effort in-effort out or flow in-flow out
Modulated Transformer	$\rightharpoonup\!\mid \underset{n(\theta)}{\overset{\downarrow\theta}{MTF}} \rightharpoonup\!\mid$	$e_2 = n(\theta)\,e_1$ $f_1 = n(\theta)\,f_2$	
Gyrator	$\vdash\!\xrightharpoonup{1} \underset{n}{GY} \xrightharpoonup{2}\!\mid$	$e_2 = n\,f_1$ $e_1 = n\,f_2$	flow in-flow out or effort in-effort out
Modulated Gyrator	$\vdash\!\rightharpoonup \underset{n(\theta)}{\overset{\downarrow\theta}{MGY}} \rightharpoonup\!\mid$	$e_2 = n(\theta)\,f_1$ $e_1 = n(\theta)\,f_2$	
CONSTRAINT NODES			
1-junction	$\xrightharpoonup{1}\!\mid 1 \xrightharpoonup{2}\!\mid$, 3	$e_2 = e_1 - e_3$ $f_1 = f_2$ $f_3 = f_2$	one flow input
0-junction	$\vdash\!\xrightharpoonup{1} 0 \vdash\!\xrightharpoonup{2}$, 3	$f_2 = f_1 - f_3$ $e_1 = e_2$ $e_3 = e_2$	one effort input

Appendix B Fuel Delivery System Parameters

Submodel	Parameter			
	Name	Value	Units	
Global	β	760	MPa	1
	ρ	737.22	kg/m^3	1
	ν	6.4×10^{-7}	m^2/s	1
	Re_L	2000		1
	Re_T	4000		1
Fuel Tank	P_T	$1.1 * P_{atm}$	Pa	2
Fuel Pump	Q_{PT}	5.28×10^{-5}	m^3/s	1
	C_P	4.11×10^{-11}	$m^3/s/Pa$	3
Fuel/Return Pipe	D	10	mm	2
	L	3.375	m	2
Pulsation Damper	A_A	0.001257	m^2	2
	k_A	15.63	kN/m	4
Fuel Rail	D	10	mm	2
	L	0.5	m	2
Fuel Injectors	C_dA_v	1.25×10^{-7}	m^2	4
Pressure Regulator	A_{RP}	0.00085	m^2	3
	A_R	0.000275	m^2	3
	B_R	2	Ns/m	2
	C_d	0.6		1
	r	3.1	mm	3
	F_0	200	N	2
	M_R	21.7	g	3
	k_R	31.5	kN/m	3

[1]Value typical to the industry
[2]Estimated value
[3]Value used from [10]
[4]Value determined through calculation

Appendix C Fuel Delivery System Element Activities

Submodel	Element	Activity	Activity Index	Cumulative Activity	Comments
Pulsation Damper	Spring Compliance	38.239	19.433%	19.433%	Required elements to maintain 98% integrity.
Fuel Rail	Rail Inertia2	33.839	17.197%	36.630%	
Fuel Rail	Rail Inertia1	23.014	11.696%	48.325%	
Fuel Rail	Rail Inertia3	22.862	11.618%	59.943%	
Fuel Rail	Fuel Incompressibility1	14.981	7.613%	67.557%	
Fuel Rail	Fuel Incompressibility2	14.853	7.548%	75.105%	
Return Pipe	Return Pipe Inertia	14.153	7.192%	82.297%	
Return Pipe	Fuel Incompressibility	12.245	6.223%	88.520%	
Pressure Regulator	Orifice Restriction	8.085	4.109%	92.629%	
Fuel Pump	C_P	7.200	3.659%	96.288%	
Fuel Rail	Fuel Incompressibility3	2.017	1.025%	97.313%	
Pressure Regulator	Spring Compliance k_R	1.595	0.811%	98.124%	
Pressure Regulator	Regulator Mass M_R	1.388	0.705%	98.829%	Required to maint 99% integrity.
Fuel Rail	Rail Resistance2	0.366	0.186%	99.015%	
Fuel Rail	Rail Resistance3	0.364	0.185%	99.200%	
Fuel Rail	Rail Resistance1	0.364	0.185%	99.386%	
Fuel Pipe	Fuel Pipe Inertia	0.309	0.157%	99.543%	
Fuel Pipe	Fuel Incompressibility	0.301	0.153%	99.696%	
Return Pipe	Return Pipe Resistance	0.190	0.097%	99.793%	
Pressure Regulator	Fuel Damping B_R	0.134	0.068%	99.861%	Retained to prevent high freq.
Fuel Pipe	Fuel Pipe Resistance	0.092	0.047%	99.907%	
Inj1	Needle Valve	0.049	0.025%	99.932%	May be retained due to interest.
Inj4	Needle Valve	0.049	0.025%	99.957%	
Inj2	Needle Valve	0.044	0.022%	99.979%	
Inj3	Needle Valve	0.041	0.021%	100.000%	

TOTAL ACTIVITY:	196.774

Appendix D Fuel Delivery System Iconic Bond Graph Model

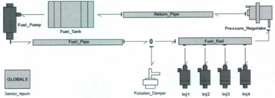

Appendix E Vehicle Model Activity Analysis for Variable Throttle, 1° Inclined Road

Submodel	Element	Activity Index	Cumulative Activity
Crankshaft	Vehicle Mass	34.4526%	34.45265%
Crankshaft	Loading	22.7763%	57.22896%
Drag	Drag	15.7735%	73.00246%
Road Load	Road Load	5.57442%	78.57688%
Crankshaft	Friction	3.98841%	82.56529%
LF Wheel	Rolling Resistance	2.47175%	85.03704%
RF Wheel	Rolling Resistance	2.47175%	87.50880%
Throttle Body	Throttle Restriction	2.04651%	89.55531%
Crankshaft	Passenger Mass	1.87514%	91.43045%
LR Wheel	Rolling Resistance	1.84024%	93.27069%
RR Wheel	Rolling Resistance	1.84024%	95.11093%
Crankshaft	Transmission Inertia	1.19435%	96.30528%
Crankshaft	Wheel Mass	0.85007%	97.15534%
Cyl1	*Cylinder Filling*	*0.51199%*	*97.66733%*
Cyl2	*Cylinder Filling*	*0.51199%*	*98.17933%*
Cyl3	*Cylinder Filling*	*0.51199%*	*98.69132%*
Cyl4	*Cylinder Filling*	*0.51199%*	*99.20331%*
Crankshaft	Engine Inertia	0.47774%	99.68105%
Crankshaft	Driveshaft Inertia	0.23039%	99.91144%
LF Strut	Strut Compliance	0.01717%	99.92861%
RF Strut	Strut Compliance	0.01717%	99.94578%
Manifold	*Manifold Filling*	*0.00724%*	*99.95303%*
LF Strut	Strut Damping	0.00668%	99.95970%
RF Strut	Strut Damping	0.00668%	99.96638%
Pressure Reg	Orifice Restriction	0.00533%	99.97171%
Fuel Pump	Pump Loss	0.00504%	99.97675%
LF Wheel	Tire Compliance	0.00484%	99.98159%
RF Wheel	Tire Compliance	0.00484%	99.98643%
P Damper	*Spring Compliance*	*0.00314%*	*99.98957%*
LF Wheel	Tire Damping	0.00139%	99.99096%
RF Wheel	Tire Damping	0.00139%	99.99235%
Fuel Rail	Rail Inertia3	0.00115%	99.99349%
Fuel Rail	Rail Inertia1	0.00115%	99.99464%
Fuel Rail	Fuel Compress1	0.00093%	99.99557%
Fuel Rail	Fuel Compress2	0.00093%	99.99651%
Return Pipe	Return Pipe Inertia	0.00082%	99.99733%
Fuel Rail	Rail Inertia2	0.00075%	99.99808%
Return Pipe	Fuel Compress	0.00059%	99.99867%
Fuel Rail	Fuel Compress3	0.00032%	99.99899%
Inj1	*Needle Valve*	*0.00016%*	*99.99915%*
Inj4	*Needle Valve*	*0.00016%*	*99.99931%*

Inj3	*Needle Valve*	*0.00016%*	*99.99947%*
Pressure Reg	Regulator Mass	0.00008%	99.99955%
Inj2	*Needle Valve*	*0.00008%*	*99.99963%*
Gearbox	In Compliance	0.00007%	99.99970%
Fuel Pipe	Fuel Pipe Resist	0.00005%	99.99975%
Return Pipe	Return Pipe Resist	0.00004%	99.99979%
Pressure Reg	Spring Compliance	0.00004%	99.99982%
Fuel Rail	Rail Resistance1	0.00003%	99.99985%
Fuel Rail	Rail Resistance2	0.00003%	99.99988%
Fuel Rail	Rail Resistance3	0.00003%	99.99991%
Gearbox	Out Compliance	0.00002%	99.99994%
Fuel Pipe	Fuel Compress	0.00002%	99.99996%
Fuel Pipe	Fuel Pipe Inertia	0.00001%	99.99997%
Gearbox	In Damping	0.00001%	99.99998%
Pressure Reg	Fuel Damping	0.00001%	99.99999%
Gearbox	Out Damping	0.00001%	100.00000%
LR Strut	Strut Damping	0.00000%	100.00000%
RR Strut	Strut Damping	0.00000%	100.00000%
LR Wheel	Tire Compliance	0.00000%	100.00000%
RR Wheel	Tire Compliance	0.00000%	100.00000%
LR Strut	Strut Compliance	0.00000%	100.00000%
RR Strut	Strut Compliance	0.00000%	100.00000%
LR Wheel	Tire Damping	0.00000%	100.00000%
RR Wheel	Tire Damping	0.00000%	100.00000%

Elements in grayed-out cells were eliminated during the MORA process.
Elements in italics should have been eliminated by MORA but were retained for their physical significance to the model.

Appendix F Complete Vehicle Model

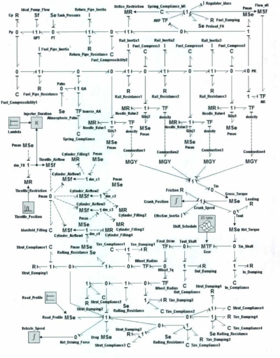

Appendix G Reduced Vehicle Model

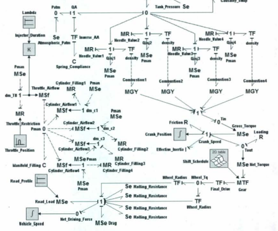

Appendix H Iconic Vehicle Model

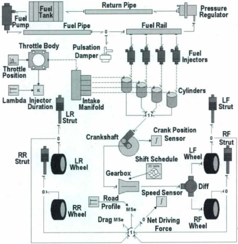

Appendix I Road-Ready Iconic Vehicle Model

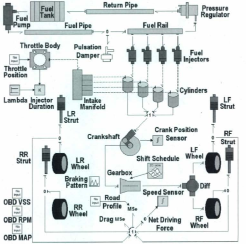

Appendix J Road-Ready Proper Vehicle Model